Utrecht University

NEWCELLS
BEST BIOLOGY DRIVING *IN VITRO* INNOVATION

The Scar-in-a-Jar

An In Vitro Renal Fibrosis Model

Dounia Sarhane

Newcells Biotech Limited

Department of the Kidney Development Team

Newcastle Upon Tyne, United Kingdom

March 27th 2023

The development of an *in vitro* disease model of glomerular renal fibrosis

Minor Research Project

Master's: Drug Innovation, Utrecht University

Author: Dounia Sarhane

Student number: 6103715

Examiner & supervisor: Dr. Kathryn Garner

Second Reviewer: Prof. dr. Roos Masereeuw

Company: Newcells Biotech Limited

Department: Kidney Development Team

Abstract

Objectives: Worldwide, hundreds of millions of individuals are known to be afflicted by chronic kidney disease (CKD). Renal fibrosis is known to be the final manifestation of CKD causing the accumulation of irreversible scarring connective tissue due to progressive maladaptive tissue injury repair. This study aims to develop an in vitro glomerular fibrosis model using human primary kidney cells. The hypothesis is that by treating primary kidney cells with fibrosis-inducing and fibrosis-reducing compounds renal fibrosis can be physiologically mimicked and reversed.

Methods: Human fibroblasts and podocytes were isolated from human kidney donors and subsequently treated for 72h with increasing concentrations of various fibrogenic inducers (Adriamycin, AngII, TGF-β1, and TNFα) in absence or presence of fibrogenic inhibitors (Nintedanib, Pirfenidone, and SB431542). The progression and reversal of renal fibrosis are assessed by quantifying the following pro-fibrotic effects: the secretion of monocyte chemoattractant protein-1 secretion (ELISA), the expression of ECM markers collagen I, collagen IV and fibronectin (immunofluorescence), and the proliferation of myofibroblast with immunofluorescence staining for αSMA.

Results: TGF-β1 was identified as a potent fibrogenic inducer causing an increase of all pro-fibrotic effects in both renal cell types. In contrast to TGF-β1, none of the other fibrogenic inducers were able to exert pro-fibrotic effects. From the fibrogenic inhibitors, SB431542 significantly attenuated TGF-β1-induced pro-fibrotic effects. Collated data showed a strong correlation between the MCP-1 levels and ECM marker expression in TGF-β1-treated renal cells.

Conclusions: This study successfully developed an in vitro renal fibrotic model which opens up new avenues for the understanding of the pathogenesis underlying renal fibrosis. Furthermore, this study makes an important first step towards a standardised and reproducible commercial model that has the potential to aid in the drug discovery of anti-fibrotic therapies and reduce the worrying risk of CKD.

Layman's Summary

Renal fibrosis is a process that occurs in patients suffering from chronic kidney disease (CKD). Worldwide, hundreds of millions people are known to be affected by CKD. Kidneys are important organs for the elimination of waste material and extra fluid transported from the blood to urine. However, these functions of the kidney are negatively impacted by renal fibrosis. Renal fibrosis namely replaces the functional kidney cells for stiff and non-functional scars. The production and increase of scarring tissue damages the kidney structure and its ability to filter the blood overtime. This will eventually lead to severe kidney failure in patients which, in the worst cases, need a kidney transplantation.

One of the most important drivers of renal fibrosis is chronic inflammation in the kidney. In case of an inflammation present in the kidney, the body's immune system starts a natural reaction to fight this inflammation. However, in the progression of renal fibrosis this natural reaction of the immune system does not stop as the inflammation in the kidney is chronic. During an immune response, immune cells and kidney cells produce various cytokines and factors that activate surrounding immune and kidney cells, such as endothelial cells, podocytes, and fibroblasts.

A cytokine that plays in important role in the progression of renal fibrosis is the transforming growth factor beta 1 (TGF-β1) that causes the production of scarring tissue via its TGF-β1 receptor/ALK-5 receptor. Other examples of important factors are tumour necrosis growth factor alpha (TNFα), the hormone angiotensin II (AngII), and the chemokine monocyte chemoattractant protein-1 (MCP-1). The production of these factors result in pro-fibrotic effects, such as the increased release of cytokines, the activation of the scarring-tissue producing cells fibroblasts and myofibroblasts, and the accumulation of scarring tissue (also known as extracellular matrix; ECM).

Although the consequences of renal fibrosis in CKD are a serious risk to patients' life, there are still no effective treatments to fight this disease. Therefore, this study attempted to develop an *in vitro* model of renal fibrosis that mimics the physiological kidney environment in the human body. The hypothesis is that such a disease model can be developed by treating kidney cells with factors that are able to induce and inhibit renal fibrosis.

To test the hypothesis, fibroblasts and podocytes were isolated from human kidney donors after which they were treated with renal fibrotic-inducing factors (AngII, TGF-β1, and TNFα) and renal

fibrotic-inhibiting drug compounds (Pirfenidone, Nintedanib, and SB431542). To assess the progression and inhibition of renal fibrosis in these cells, the following three pro-fibrotic effects were analysed: 1) the release of MCP-1; 2) the production of ECM; and 3) the proliferation of myofibroblasts.

The results of this study demonstrate two important things. First, TGF-β1 can be considered as a potent inducer of renal fibrosis as it resulted in all three pro-fibrotic effects. Second, the pro-fibrotic effects induced by TGF-β1 were reversed by the drug compound SB431542. Based on these results, it can be concluded that this study was able to develop an *in vitro* model for renal fibrosis. The development of this model will help in the understanding of the processes underlying renal fibrosis and the development of potential new drug treatments to reduce the worrying risk of CKD.

Acknowledgements

My main gratitude goes to Kathryn for her great assistance with and guidance through this research project. She gave me the opportunity and freedom to learn new techniques and skills in the laboratory. Additionally, I want to thank her for putting trust in me and giving me the opportunity to develop an independent work attitude. Further, I would like to thank the rest of the kidney development team members for their great help and discussion concerning the findings of this study. Their enthusiasm and advices were of great help. Lastly, I want to thank Newcells Biotech for the pleasant and motivating work environment.

List of Abbreviations

ALK-5	Activin receptor-like kinase 5
AngII	Angiotensin II
CKD	Chronic kidney disease
DAPI	4',6-Diamidino-2-phenylindole, dihydrochloride
ECM	Extracellular matrix
ELISA	Enzyme-linked immunoassay
EMT	Epithelial-mesenchymal transition
FBS	Fetal bovine serum
FGM-2	Fibroblast growth medium-2
FSP-1	Fibroblast-specific protein-1
GADPH	Glyceraldehyde-3-phosphate dehydrogenase
IF	Immunofluorescence
IPF	Idiopathic pulmonary fibrosis
MACS	Magnetic Activated Cell Sorting
MCP-1	Monocyte chemoattractant protein-1
MeOH	Methanol
MPS	Microphysiological system
NGS	Normal goat serum
NHS	National Health System
NME	New molecular entity
PBS	Phosphate buffer solution
RT-PCR	Reverse transcription polymerase chain reaction
TGF-β	Transforming growth factor beta
TNF-α	Tumour necrosis growth factor alpha

Contents

Abstract 3
Layman's Summary 4
Acknowledgements 6
Introduction 9
Materials and Methods 13
Results 18
Discussion 32
Conclusion 36
Supplementary 37
References 45

Introduction

Chronic kidney disease

Worldwide, more than 800 million individuals are known to be afflicted by chronic kidney disease (CKD), of which approximately 1.2 million lives were being claimed in 2017 globally (Bikbov et al., 2020). This long-term progressive condition, characterised by a gradual functional loss of the kidney, represents a serious hazard to human health accounting for a large burden especially in low- and middle income countries (Kovesdy, 2022). While the early CKD stages are asymptomatic, people who have been diagnosed with CKD will eventually develop a wide range of symptoms that will necessitate dialysis or a kidney transplant in the later stages (Liu, 2006).

Literature has shown a growing evidence for a higher susceptibility to CKD in adult older than 70 years associated with higher morbidity and mortality. Given the poor long-term prognosis and rising annual incidence, which is in part driven by the ageing population, this increased susceptibility is concerning (Cañadas-Garre et al., 2019; Mallappallil et al., 2014). CKD patients clinically manifest with hypertension, cardiovascular dysfunction, and (chronic) inflammation. In spite of the severity of this problem, CKD patients still suffer from a lack of effective treatments, and more must be done to tackle this (Liu, 2011).

Despite its diversity in aetiologies, diabetes and hypertension are known to be the two principal contributors to CKD that may culminate in elevated glomerular capillary pressure and persistent renal tissue injury. Other risk-inducing factors include infectious glomerulonephritis, renal vasculitis, ureteral obstruction, and chronic environmental exposures to air pollutants and toxins (Tsai et al., 2021; Vaidya & Aeddula, 2022).

Renal fibrosis

The final manifestation of CKD is often attributed to the presence of the common pathogenesis renal fibrosis. Renal fibrosis, evidenced by an imbalance between excessive synthesis and reduced degradation of extracellular matrix (ECM), can be considered as the histological end-point of progressive maladaptive repair of kidney tissue injury (Nogueira et al., 2017). The kidney is structurally a complex organ that can be histologically classified as glomeruli, tubulointerstitium, and vessels (Bülow & Boor, 2019). Among these compartments, a wide variety of renal cell types are known to be involved in this maladaptive repair process, including epithelial cells (podocyte and parietal epithelial cells), glomerular endothelial cells, and mesenchymal cells (myofibroblasts and fibroblasts) (Panizo et al., 2021).

Each histologically distinct compartment exhibits different pathological features of renal fibrosis, including tubulointerstitial fibrosis, glomerulosclerosis, vascular sclerosis, and the loss of renal parenchyma (Pinto et al., 2017). The accumulation of disproportional deposition of fibrotic matrix disrupts the kidney architecture by replacing parts of the functional tissue within the renal parenchyma with irreversible scarring connective tissue (**Figure 1**). As a consequence of this gradual tissue remodelling, the renal blood flow decreases leading to progressive kidney function decline and inevitably to renal failure (Efstratiadis et al., 2009; Panizo et al., 2021).

Different stimuli are known to trigger the process of renal fibrosis, such as trauma, infection, metabolic disorders, autoimmunity, and (chronic) inflammation. The latter is recognised as an important driver of the progression of renal fibrosis in CKD (Panizo et al., 2021).

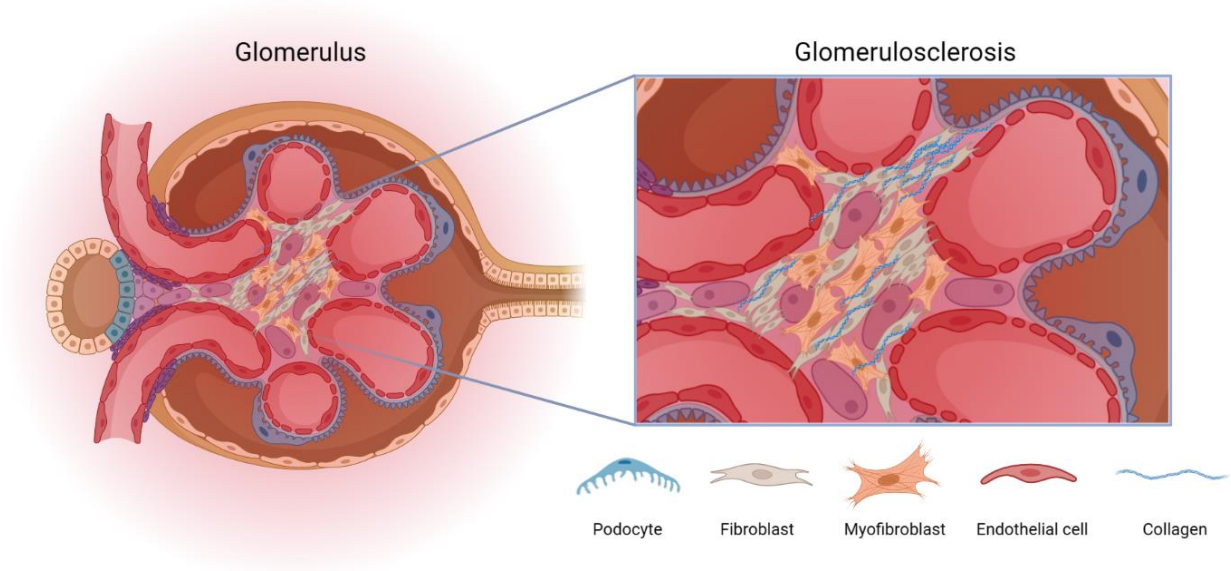

Figure 1: The histological effect of glomerulosclerosis. The figure gives an overview of the progression of renal fibrosis in the glomerulus resulting in glomerulosclerosis. Glomerular fibrotic lesions, referred to as glomerulosclerosis, consist of accumulated fibroblasts and myofibroblasts causing the excessive deposition of extracellular matrix (ECM) components, such as collagen. This excessive ECM deposition replaces functional tissue and disrupts the kidney architecture. (Created with Biorender)

Inflammation

Renal endothelial and epithelial cells release pro-inflammatory mediators during an innate inflammatory response, among them the chemokine monocyte chemoattractant protein-1 (MCP-1), which stimulates the migration and invasion of leukocytes to the site of tissue injury and infection (Guerrot et al., 2012). Recruited inflammatory cells produce a wide variety of pro-inflammatory and pro-fibrogenic factors which subsequently provoke the prolonged activation and accumulation of renal podocytes, fibroblasts and myofibroblasts. Examples of pro-fibrogenic factors are interleukin-8 (IL-8), transforming growth factor beta (TGF-β), and tumour necrosis factor alpha (TNF-α) (Lv et al.,

2018). The activated fibroblasts, known as critical pro-fibrotic cells, are responsible for the excess synthesis of ECM components, such as collagen I, collagen III, collagen IV, and fibronectin. The synthesis of these components contribute to the development of interstitial and glomerular fibrosis (**Figure 1**) (Black et al., 2019; Bülow & Boor, 2019). The above discussed innate response is illustrated in the figure below.

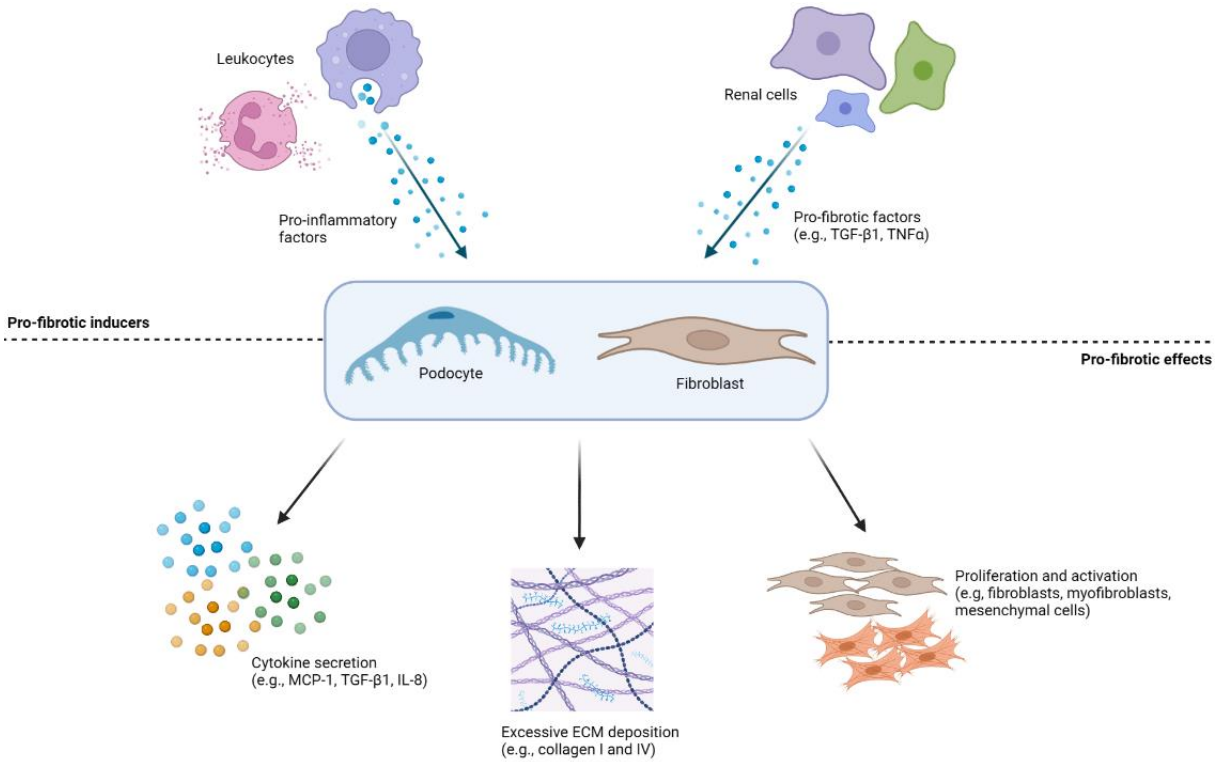

Figure 2: Fibrotic innate inflammatory response. This figures represents the pro-fibrotic inducers and effects present during an inflammatory response in renal fibrosis. Leukocytes and renal cells produce various pro-inflammatory and pro-fibrotic factors that activate renal cells, among them podocytes and fibroblasts. The activation of these renal cells results in the following pro-fibrotic effects: the secretion of various cytokines, the excessive synthesis of extracellular matrix components, and the proliferation and activation of (myo)fibroblasts and mesenchymal cells. ECM, extracellular matrix; IL-8, interleukin-8; MCP-1, monocyte chemoattractant protein-1; TGF-β1, transforming growth factor beta-1; and TNFα, tumour necrosis factor alpha. (Created with BioRender)

Transforming growth factor beta

The cytokine TGF-β is considered as a primary mediator of renal fibrosis, with its isoform TGF-β1 playing a crucial role in the deterioration of kidney tissue. TGF-β1 is widely expressed by renal cells and infiltrating leukocytes which triggers a self-sustaining autocrine loop of fibrotic effects through TGF-β type I receptor/activin receptor-like kinase 5 (ALK-5) signalling (Eddy, 2011). The TGF-β/Smad signalling pathway contributes to the progression of renal fibrosis by promoting various fibrotic processes. These include: 1) the stimulation of (myo-)fibroblast proliferation and activation; 2) the stimulation of ECM production; 3) the inhibition of ECM degradation by suppressing matrix-degrading proteinases; and 4) the promotion of epithelial-mesenchymal transition (EMT), which causes the transdifferentiation of epithelial cells into myofibroblasts (Borthwick et al., 2013; Meng et al., 2015).

Studies have demonstrated the interaction between TGF-β1 and the renin-angiotensin system (RAS). Angiotensin II, the primary hormone of the RAS, activates its Angiotensin II type 1 receptor 1 (AT1), which triggers a series of intracellular signalling pathways that causes the expression of TGF-β1 and its receptor (Mezzano et al., 2001; Murphy et al., 2015).

Renal fibrotic microphysiological system model

Microphysiological systems (MPS) models are currently actively developed to provide preclinical screening of drugs and/or new molecular entities (NMEs). These *in vitro* (disease) models have the capacity to recapitulate the physiological environment more accurately and therefore anticipated to better predict drug toxicity and mechanism, and aid in the understanding of disease pathogenesis. Furthermore, the scientific implementation of MPS models fosters the necessity and capability to circumvent animal testing in the field of drug development (Chen et al., 2021).

This study is designated to establish a standardised and reproducible *in vitro* disease model of renal fibrosis of the glomerulus exerting relevant pro-fibrotic biomarkers by using human primary kidney cells. The outcomes of this study will be used to answer the following research questions: 'To what extent is the developed kidney MPS disease model able to mimic the physiological environment of glomerular fibrosis? And to what extent can the fibrotic effects of this disease model be reversed?'.

The hypothesis presented in this thesis is that by treating the primary kidney cells with fibrosis-inducing compounds (e.g., TGF-β1, TNF-α, and AngII) and fibrosis-reducing compounds the presence of relevant pro-fibrotic markers, contributing to renal fibrotic progression, can be physiologically mimicked and reversed. By addressing the aforementioned questions, the outcomes of this study will necessitate in the understanding of the underlying development of renal fibrosis, the acceleration of drug discovery, and the development of a commercially available disease model. These insights are valuable since, as of today, the exact mechanism implicated in renal fibrosis remains poorly understood – whilst, despite the persistent rising burden, no specific therapeutic options have been established yet (Prakoura et al., 2019).

Materials and Methods

Isolation of renal podocytes and fibroblasts from human kidney cortexes

Cortex dissection

Kidney samples from human donors were provided by tissue banks, which had obtained appropriate ethical approval for use in research. The kidney cortex surface layers were minced into small pieces with sterile scalpels and weighed to determine the total amount of tissue in grams. The total amount of tissue was equally distributed between 50 mL tubes resulting in 5-7 grams tissue per tube. Next, tissue was resuspended in isolation medium (**Table 1: Kidney isolation medium**) and incubated with 200 uL Collagenase type II per 1 gram tissue overnight. Digested cell mixture was passed through a 40 µm cell strainer (Brown et al., 2008).

Table 1: Kidney isolation medium

Reagent	Source	Cat. No	(v/v)
RPMI-1640 Medium with L-glutamine and sodium bicarbonate	Merck Life Sciences	R8758	-
Fetal Bovine Serum	Gibco; Thermo Fischer Scientific	10270106	5%
Penicillin/Streptomycin	Life Technologies; Thermo Fischer Scientific	15140122	1%

Supplements of the kidney isolation medium with volume concentrations are mentioned.

Human podocytes expansion

To collect the contents of the cell strainers, the strainers were washed with isolation medium until little is left on top of the strainers. The cell suspensions were combined, resuspended in isolation medium, and were transferred to a T150 flask (t=0; passage 0). The following day (t=1), the floating glomeruli were sub-divided into multiple T25 flasks in podocyte growth medium (**Table 2**). The podocytes are the first cells to grow out of from the glomeruli as previously described (Ni et al., 2012; Saleem et al., 2002).

After reaching 80% confluency in the T25 flasks (t=3-4), cells were washed with PBS and incubated with TrypLE express enzyme (Gibco; Thermo Fischer Scientific, NY, US) and subsequently quenched with podocyte growth medium. After centrifugation (1200 rpm for 5 min), the remaining pellet was resuspended in podocyte growth medium and cells were then counted using 0.4% Trypan Blue solution (VWR, PA, USA) and the LUNA-II Automated Cell Counter (Logos Biosystems, KR). Finally, podocytes (passage 1) were seeded into black wall 96-well microplate (Corning, NY, USA) a seeding density of 5000 per well.

Table 2: Podocyte growth medium

Reagent	Source	Cat. No	(v/v)
RPMI-1640 Medium with L-glutamine and sodium bicarbonate	Merck Life Sciences	R8758	-
Fetal Bovine Serum	Gibco; Thermo Fischer Scientific	10270106	10%
Penicillin/Streptomycin	Life Technologies; Thermo Fischer Scientific	15140122	1%

Supplements of the podocyte growth medium with volume concentrations are mentioned.

Human fibroblasts expansion

To isolate renal fibroblasts, centrifugation was performed on the strained cell suspension for 10 min at 1200 rpm on the day of kidney isolation (t=0) immediately following straining. The pellet was resuspended in isolation medium and subsequently loaded onto a discontinuous Percoll density gradient (Thermo Fischer Scientific, MA, USA). The top layers of the Percoll gradient suspensions, in which human fibroblasts are localised, were centrifuged for 10 min at 1200 rpm. The pellet was resuspended in fresh isolation medium and centrifuged for 10 min at 1200 rpm once more. The yielded pellet was diluted in fibroblast growth medium (**Table 3**) and seeded into T25 flasks (Thermo Fischer Scientific, MA, USA).

Table 3: Fibroblast growth medium

Reagent	Source	Cat. No	(v/v)
Fibroblast Basal Medium (FBM)	Lonza Biosciences	CC-3131	-
Fibroblasts Growth Medium-2 (FGM-2) Single Quots	Lonzo Biosciences	CC-4126	-

Supplements of the fibroblast growth medium are mentioned.

Magnetic activated cell sorting of human renal fibroblasts

Magnetic activated cell sorting (MACS) was performed to separate fibroblasts from epithelial cells contaminating the culture. The magnetic separation was carried out using the MidMACS Separator with LS MACS columns (Miltenyi Biotec, DE). After reaching 90% confluency in the T25 flasks, cells (passage 0) were washed with PBS and incubated with TrypLE express enzyme (Gibco; Thermo Fischer Scientific, NY, US) and subsequently quenched with fibroblast growth medium. After centrifugation (1200 rpm for 5 min), the remaining pellet was resuspended in MACS buffer and cells were then counted using 0.4% Trypan Blue solution (VWR, PA, USA) and the LUNA-II Automated Cell Counter

(Logos Biosystems, KR). The cell suspension, consisting of a maximum of 10^8 cells, was centrifuged at 1200 rpm for 5 min after which the pellet has been resuspended in 800 µL MACS buffer.

Fibroblasts were purified by incubating the single cell suspension with 200 µL Anti Human Fibroblast-Specific Protein-1 (FSP-1) MicroBeads (Miltenyi Biotech, DE) for 30 min in the dark on ice. Cells were then washed with MACS buffer and subsequently centrifuged at 1200 rpm for 5 min. After rinsing the column with the buffer, the pellet was resuspended in MACS buffer and loaded onto the column. The flow through was discarded. Next, three washes of the column with MACS buffer were performed, with each flow through being discarded. To collect the magnetic labelled fibroblasts, the column was removed from the magnetic separator while the cells were flushed out with MACS buffer and using a plunger. The flow through was collected and subsequently centrifuged for 10 min at 1200 rpm. Finally, the pellet was resuspended in FGM-2 medium and cells (passage 1) were seeded into black wall 96-well microplates (Corning, NY, USA) with a density of 5000 cells per well.

Fibrosis-inducing and -reducing treatments

Fibroblasts and podocytes were treated with pro-fibrotic markers after reaching 90% confluency in the microplates. Fibrotic-induced treatments were performed for 72 hours using different concentrations of the following fibrotic-inducing compounds: Adriamycin (Tocris Biosciences, UK; 50mM), AngII (Sigma-Aldrich, MO, USA; 10mM), TGF-β1 (R&D Systems, MN, USA; 50 µg/mL), and TNFα (Tocris Bioscience, UK; 100 µg/mL). In an attempt to inhibit the fibrotic effects, cells underwent a 1 hour treatment, before being treated with the fibrosis-inducing compounds. The following fibrosis-reducing compounds were used at one concentration: 100 µM Pirfenidone (TGF-β inhibitor; Cambridge Bioscience, UK) and 1 µM SB431542 (selective TGF-β1 receptor/ALK-5 inhibitor; Tocris Bioscience, UK). Both the fibrotic-inducing and -reducing compounds for fibroblasts and podocytes were diluted in fibroblast growth medium and 0.1% FBS RPMI-1640 supplemented with Penicillin/Streptomycin, respectively. All compounds and concentrations were tested in two technical and three biological repeats.

Quantification of MCP-1 secretion

The secreted levels of the chemoattractant MCP-1 was measured in the media collected after pro-fibrotic treatment of fibroblasts. The MCP-1 quantitation was performed using the Human CCL2/MCP-1 DuoSet ELISA kit (R&D Systems, MN, USA), according to the manufacturer's protocol. All individual samples were diluted 40-fold and assayed in triplicate. The results of the sandwich ELISA were depicted as picograms MCP-1 per mL conditioned media.

High content imaging and quantification

Immunofluorescence staining was carried out on cultured human podocytes to enable the visualisation of *in vitro* renal fibrosis development. After 72 hours of pro-fibrotic treatment and media collection, the cultures were fixed with ice-cold 4% paraformaldehyde for 5 min at 4 °C. Thereafter, ice-cold permeabilization buffer containing 100% MeOH was added to the cells for 5 min at -20 °C . Following that, cells were blocked for 60 min in blocking buffer composed of 5% normal goat serum (NGS) (v/v) in PBS. Primary antibodies that were diluted in 1% NGS (v/v) in PBS were then added to the cells and incubated for 2 hours on the rocker. Subsequent to the incubation, cells were washed 3 times with PBS followed by 60 min incubation with secondary antibodies in 1% NGS (v/v) in PBS, in the dark while being rocked at room temperature. Three PBS washing steps were performed with a following incubation with DAPI, in PBS, at room temperature with rocking for 10 min. Finally, cells were washed twice with PBS of which the second wash being left on the cells to allow for imaging. In the table below, all antibodies with dilution factors are listed (**Table 4**).

Table 4: Primary and secondary antibodies

Antibodies	**Source**	**Cat. No**	**Dilution**
Rabbit anti-α-smooth muscle actin	Cell Signaling Technology	19245	1:200
Rabbit anti-collagen IAI	Cell Signaling Technology	72026	1:200
Rabbit anti-collagen IV	Abcam	GR3448024-1	1:200
Rabbit anti-fibronectin	Cell Signaling Technology	26836	1:200
Rabbit anti-podocin	Sigma-Aldrich	069M4836V	1:200
Alexa Fluor 488 goat anti-rabbit IgG	Invitrogen	A11008	1:200
Rabbit anti-fibroblast specific protein (FSP) 1	Abcam	GR3246704-1	1:200
DAPI (1.5 µM)	Sigma-Aldrich	D9542	1:5000

All antibodies with dilution factors are summarised.

High content imaging was performed using the ImageXpress Pico Automated Cell Imaging System with channels for DAPI and Alexa Fluor 488 nm. Four different loci per well were acquired with a 10X objective lens. Imaging settings were kept the same for all biological repeats to ensure reliable and

comparable quantification. Subsequently, protein expressions were semi-automatic quantified by means of the PICO high-content imaging analysis software. Detailed image analysis settings can be found in the table below (**Table 5**).

Table 5: PICO High-content imaging protein expression analysis settings.

Channel	Intensity	Minimum Width	Maximum width
DAPI	50	5	65
Biomarker	50	5	100

Statistical analysis

Statistical analyses were conducted using GraphPad Prism 9.0 (GraphPad Software, CA, USA). All data are expressed as mean and standard error mean (SEM) of the biological repeats. Two-Way ANOVA was used to analyse continuous differences between fibrosis-inducing treatments with and without pharmacological inhibitors in terms of mRNA expression, protein expression, and cytokine secretion. Differences between treatment concentrations were analysed by means of One-Way ANOVA. Shapiro Wilk test was used to determine the normal distribution. In case of non-parametric results, the Mann-Withney U test was used to compare treatment conditions. Associations between continuous variables were analysed with simple linear (Pearson's correlation) and nonlinear regression analyses. Results were considered significant when p-values were 0.05 or lower.

Results

Well-validated human kidney isolation method. The development of a kidney MPS model for glomerular fibrosis utilising primary kidney cells was one of the main objectives of this study. Prior to the start of this study, the established kidney isolation method of human fibroblasts and podocytes were validated by means of flow cytometry and immunostaining, respectively. The validation results present data on characterisation of isolated human renal fibroblasts and podocytes using a subset of fibroblasts- and podocyte-specific markers (**Figure 3**). The results clearly demonstrate and confirm that the established isolation method successfully isolates fibroblast and podocytes from the kidney cortex. Hence, substantiating the reliability of the isolated renal cells performed via this method in this study.

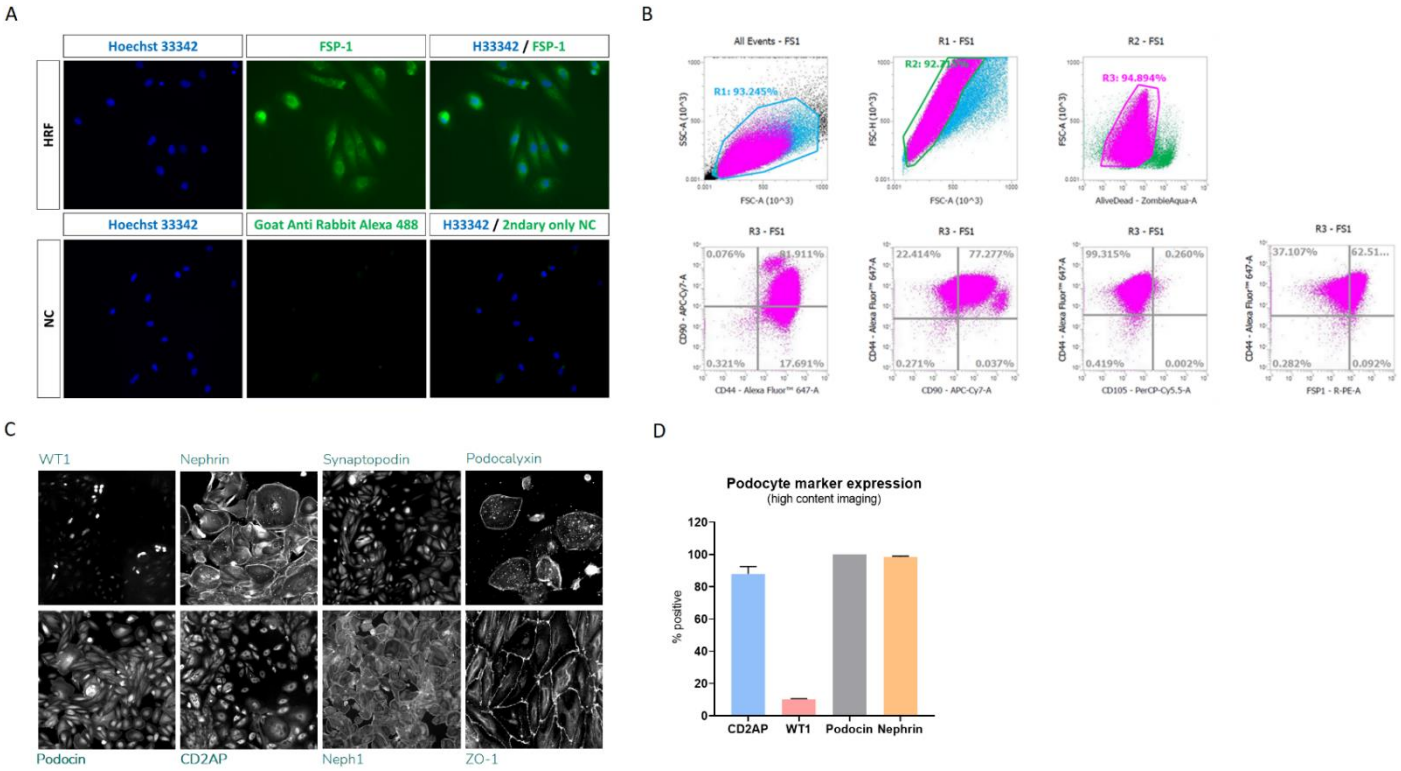

Figure 3: Characterisation of fibroblasts and podocytes isolated from human kidneys. **A|** Fluorescent microscopy images of MACS-isolated human renal fibroblasts on glass coverslips showing positivity for FSP-1, including "secondary antibody only" negative control. **B|** Flow cytometry dot plots and histograms representing the percentages of cells isolated via MACS FSP1+ showing positive staining for mesenchymal markers. Cells at passage 0 double positive: CD44+ CD90+ 81.911%; CD44+ CD105+ 0.260%; CD44+ FSP1+ 62.51%. **C|** Fluorescent microscopy images of isolated human podocytes stained for podocyte markers: CD2AP (CD2 Associated Protein), Nephrin, Neph1, Podocalyxin, Podocin, Synaptopodin, WT1 (Wilms' Tumor suppressor gene 1), and ZO-1 (Zonula Occludens-1). **D|** Quantification of podocyte marker expression using high content imaging. Error bars showing standard deviation (D). Data generated by E. Tasinato (A,B). Data generated by B. Coker and P. Singh (C, D).

Adriamycin not suitable as a positive fibrotic control. To recapitulate renal fibrosis, fibrotic-inducing treatments using Adriamycin, AngII, TGF-β1, and TNFα were performed. One of the readouts to quantify the development of renal fibrosis, induced by the treatments, is the protein expression of the following key pro-fibrotic markers performing immunofluorescence (IF): αSMA, collagen I, collagen IV, and fibronectin. The results are expressed in relative positive integrated intensity taking both the control and the area of the fluorescence signal into account.

To aid in the investigation of the treatment effects on the expression of biomarkers, optimisation experiments were carried out. These experiments include optimisation of the IF permeabilization method and the cell seeding density. Optimisation results can be found in the supplementary (**Supplementary figure 1-2**). Analysis of the data revealed that permeabilizing with 100% methanol (MeOH) overall resulted in the highest positive integrated intensity and the best staining pattern in fibroblasts. In terms of the cell seeding density, there was no difference observed in immunofluorescence signal between 5000 and 13000 cell seeding density in podocytes. In light of these findings, primary kidney cells were seeded out with a density of 5000 cells per well and cells were permeabilised using 100% MeOH for the rest of the experiments.

In an attempt to create a positive control for fibrotic-inducing treatments, fibroblasts were treated with the nephrotoxic compound Adriamycin. The hypothesis posits that by treating the primary kidney cells with the nephrotoxic compound, and therefore developing Adriamycin-induced renal fibrosis, the expression of pro-fibrotic biomarkers will significantly increase in fibroblasts.

As shown in **Figure 44,** the results of this experiment are not consistent with what was originally proposed. Adriamycin had namely no effect on collagen I and αSMA protein expression. In contrast, the fibrotic marker expression of fibronectin and collagen IV were significantly increased when fibroblasts were treated with Adriamycin concentrations of 3 µM and higher (**Figure 4E-H**). Interestingly, the protein expression of fibronectin and collagen IV does not follow a linear curve, but show a decline, subsequent to exposure to the highest concentration of Adriamycin (10 µM). Comprehensive analysis of individual images led to the finding that Adriamycin most likely causes cell apoptosis of fibroblasts because of observed nuclei reduction (**Supplementary figure 3**). Due to the lack of pro-fibrotic effects of Adriamycin on collagen I and αSMA, Adriamycin cannot be considered as a suitable positive control for fibrotic-inducing treatments in this model.

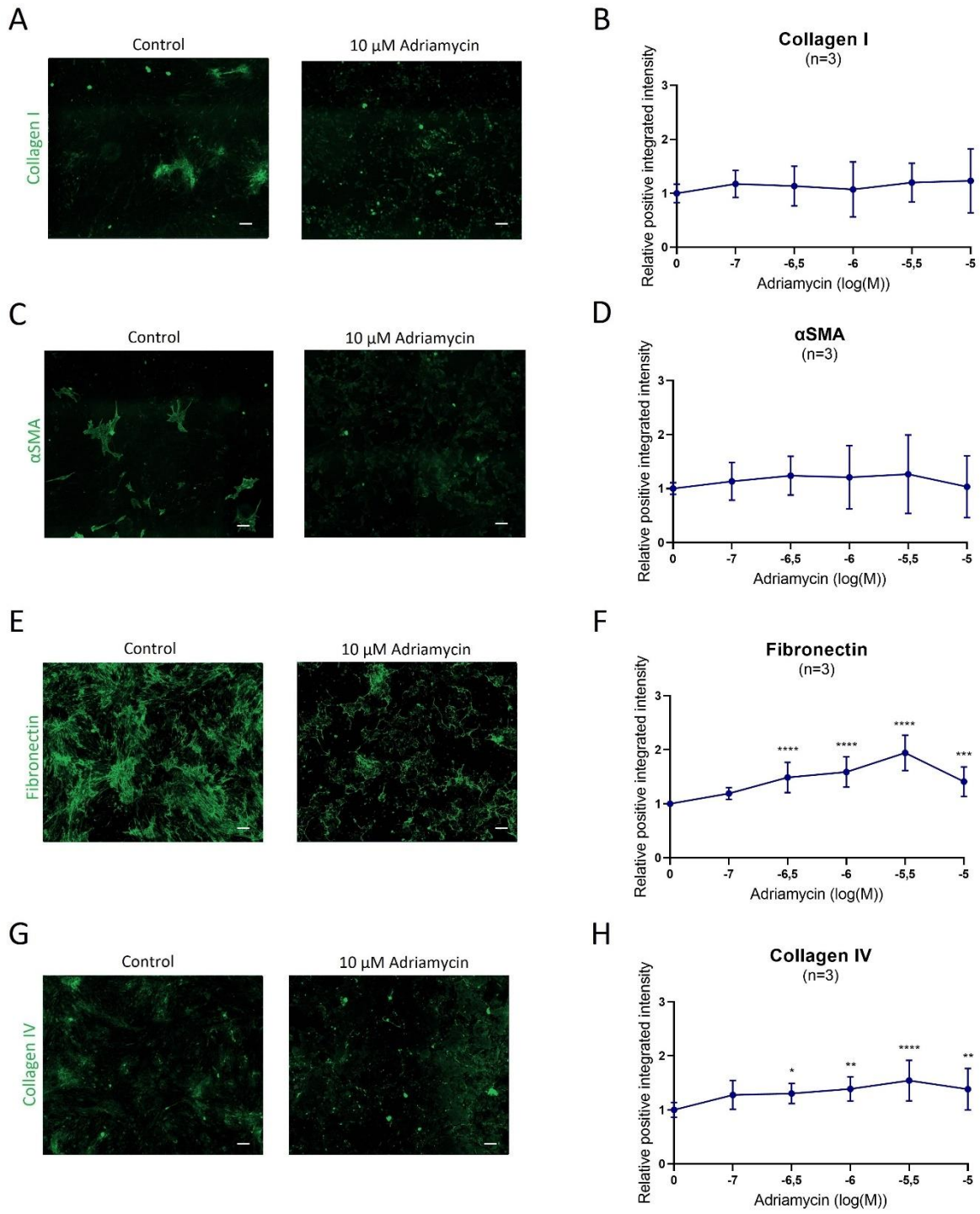

Figure 4: The histological effects of Adriamycin treatment in human fibroblasts. **A, C, E, G|** Immunofluorescence with antibodies against, collagen I, αSMA, fibronectin, and collagen IV, respectively. Protein expression of the biomarkers collagen IV and fibronectin are significantly increased when treated with 10 µM Adriamycin as compared to the control. **B, D, F, H|** Image intensity analysis for collagen I, αSMA, fibronectin, and collagen IV treated with increasing concentrations of Adriamycin. Results are expressed as relative positive integrated intensity. Statistical analysis by One-Way ANOVA (B, D, F, and H), *P<0.05, **P<0.01, ***P<0.001, ****P<000.1. Errors bars showing standard deviation. n = 3. The scale bar is 135 µm.

TGF-β1 acts as a potent driver of pro-fibrotic marker expression. The results of the TGF-β1 treatment in fibroblasts revealed promising results (**Figure 5**). Increased concentrations of TGF-β1 led to significantly higher protein expression levels of three fibrotic biomarkers: collagen I, fibronectin, and collagen IV (**Figure 5B**, **F**, and **H)**. The increase of protein levels of these markers were also visibly observable (**Figure 5A**, **E**, and **G)**. Hence, demonstrating a clear dose-response effect between pro-fibrotic marker expression and TGF-β1, with the exception of αSMA (**Figure 5C-D**). Image intensity analysis revealed that TGF-β1 treatment shows the largest effect on fibronectin accounting for a 2-fold increase of protein expression, followed by collagen IV (1,7-fold increase) and collagen I (1,4-fold increase)(**Figure 5**; right graphs). The graph trends of all markers indicate a non-linear correlation with a gradual increase of protein expression followed by a plateau phase at higher treatment concentrations. Remarkably, the results of the three biological repeats (n=3) show large error bars, whereas these large error bars are absent when looking at the data of individual donors (data not shown).

Unlike the fibrogenic inducer TGF-β1, treating fibroblasts with increasing concentrations of AngII and TNFα did not result in the hypothesised pro-fibrotic effects. None of the fibrotic markers showed differential protein expression upon treatment with AngII or TNFα in fibroblasts. The results are presented in the supplementary (**Supplementary figure 4-5**). Due to lack of pro-fibrotic effects, AngII and TNFα treatment were not carried out in podocytes.

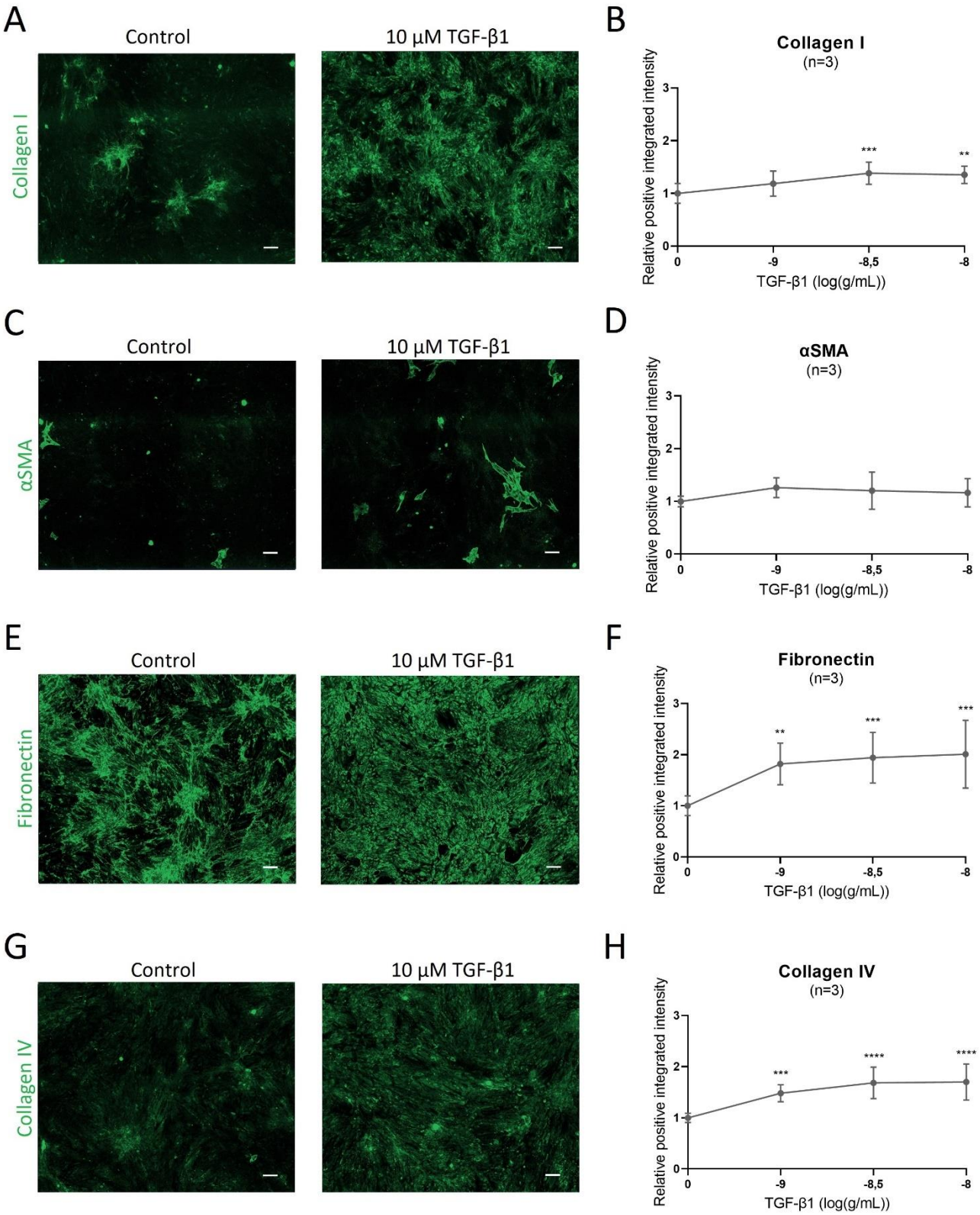

Figure 5: The histological effects of TGF-β1 treatment in human fibroblasts. **A, C, E, G|** Immunofluorescence with antibodies against, collagen I, αSMA, fibronectin, and collagen IV, respectively. Protein expression of the respective biomarkers are significantly increased when treated with 10 µM TGF-β1 as compared to the control, with the exception of αSMA. **B, D, F, H|** Image intensity analysis for collagen I, αSMA, fibronectin, and collagen IV treated with increasing concentrations of TGF-β1. Results are expressed as relative positive integrated intensity. Statistical analysis by One-Way

ANOVA (B, D, F, and H), *P<0.05, **P<0.01, ***P<0.001, ****P<000.1. Errors bars showing standard deviation. n = 3. The scale bar is 135 µm.

The results of the TGF-β1 treatment in podocytes were interestingly very similar to the results observed in fibroblasts. However, in contrast to fibroblasts, all four fibrotic biomarkers showed significantly differential protein levels with increasing TFG-β1 concentrations in podocytes. This observable increase is shown in **Figure 6** (left images) when comparing the control group with podocytes treated with 10 µM TGF-β1. According to image intensity analysis, the largest effect of TGF-β1 treatment was on fibronectin accounting for a 2,7-fold increase of protein expression, followed by collagen IV (1,9-fold increase), collagen I (1,7-fold increase), and αSMA (1,4-fold increase) (**Figure 6***Figure 6*; right graphs), about equal to what is shown in fibroblasts. Whereas TGF-β1 treatment in fibroblasts results in a clear non-linear trend, this relationship is more difficult to conclude from the dose-response graphs in podocytes.

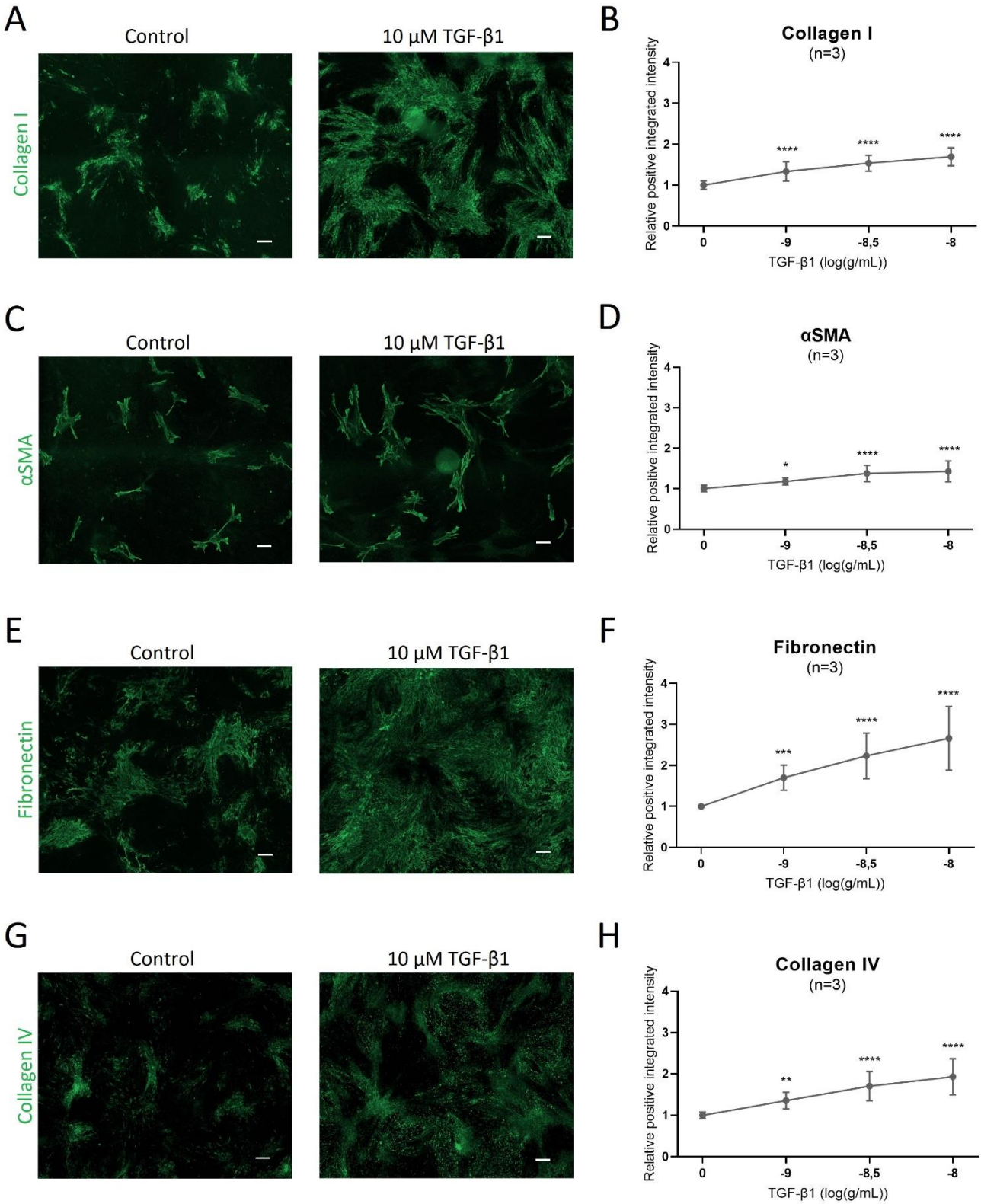

Figure 6: The histological effects of TGF-β1 treatment in human podocytes. **A, C, E, G|** Immunofluorescence with antibodies against, collagen I, αSMA, fibronectin, and collagen IV, respectively. Protein expression of the respective biomarkers are significantly increased when treated with 10 µM TGF-β1 as compared to the control. **B, D, F, H|** Image intensity analysis for collagen I, αSMA, fibronectin, and collagen IV treated with increasing concentrations of TGF-β1. Results are expressed as

relative positive integrated intensity. Statistical analysis by One-Way ANOVA (B, D, F, and H), *P<0.05, **P<0.01, ***P<0.001, ****P<000.1. Errors bars showing standard deviation. n = 3. The scale bar is 135 µm.

Renal fibrotic inducer causes morphological changes in fibroblasts and podocytes. Besides the influence of TGF-β1 on protein expressions, the morphology of both fibroblasts and podocytes showed signs of morphological changes as a response to increasing TGF-β1 concentrations. The figure below compares control cells with cells treated with the highest concentration of TGF-β1 (10 µM) (**Figure 7**). The histological changes that can be observed in fibroblasts (**Figure 7A**) and podocytes (**Figure 7B**) include: larger cell surfaces, enlarged nuclei, and less dense clusters of nuclei.

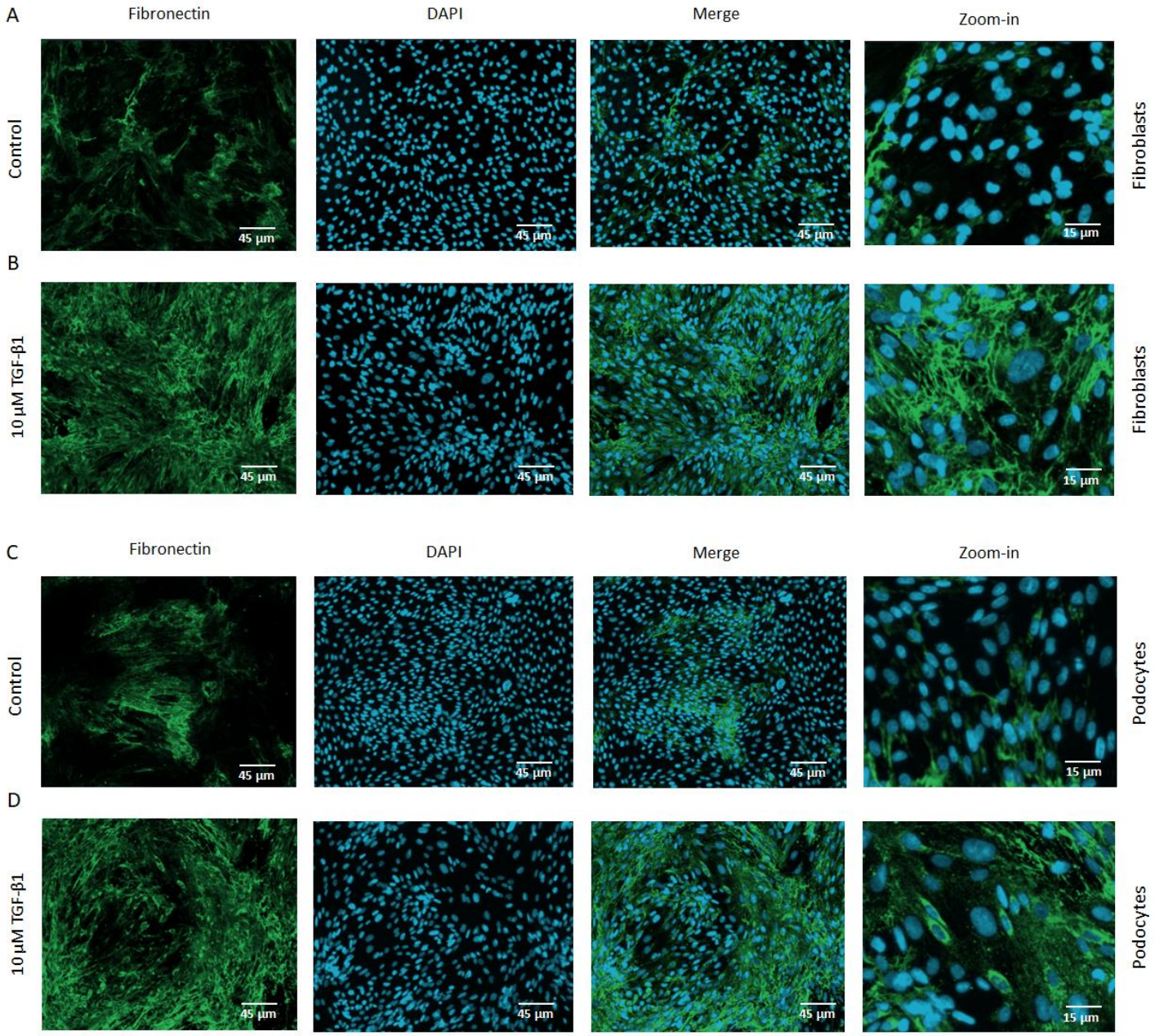

Figure 7: Morphological changes upon TGF-β1 treatment. **A, B|** Immunofluorescence staining of human fibroblasts. Human fibroblasts were stained with antibodies against fibronectin (green) and DAPI (blue) to show the differential presence of extracellular fibronectin and the size of the nuclei, respectively. The images are shown for fibroblasts without TGF-β1 treatment (**A;** control) and treated with 10 µM TGF-β1 (**B**). **C, D|** Immunofluorescence staining of human podocytes. Human

podocytes were stained with antibodies against fibronectin (green) and DAPI (blue) to show the differential presence of extracellular fibronectin and the size of the nuclei, respectively. The images are shown for podocytes without TGF-β1 treatment (**C**; control) and treated with 10 µM TGF-β1 (**D**). The scale bar is 45 µm for fibronectin, DAPI, and overlay. The scale bar is 15 µm for zoom-in.

MCP-1 levels increased upon treatment with fibrogenic inducers. As mentioned earlier, a wide range of cytokines are known to be involved in the initiation and progression of renal fibrosis. For this study, the MCP-1 secretion, responsible for the leukocyte recruitment, by TGF-β1- and Adriamycin-treated fibroblasts was investigated. First, ELISA optimisation experiments were carried out in fibroblasts to determine the optimal sample dilution using the hyperbolic regression method. From the analysis, it could be concluded that the 1:40 dilution was the most optimal dilution. Hence, this dilution factor was used to perform subsequent ELISA experiments. The optimisation results can be found in the supplementary (**Supplementary figure 6**).

As depicted in the graphs below, MCP-1 levels were increased by Adriamycin and TGF-β1 by a dose-dependent manner (**Figure 8**). Although a clear increase in MCP-1 secretion is observable, no significant increases were found in any of the treatments. Despite Adriamycin being a nephrotoxic compound, lower levels of MCP-1 were observed in fibroblasts compared to TGF-β1 treatment (**Figure 8A-B**). This finding is another indication that Adriamycin might not serve as a suitable positive control for this kidney MPS model. Whereas the MCP-1 levels gradually increases in fibroblasts and podocytes upon TGF-β1 treatment, fibroblasts treated with Adriamycin show a biphasic dose-response curve.

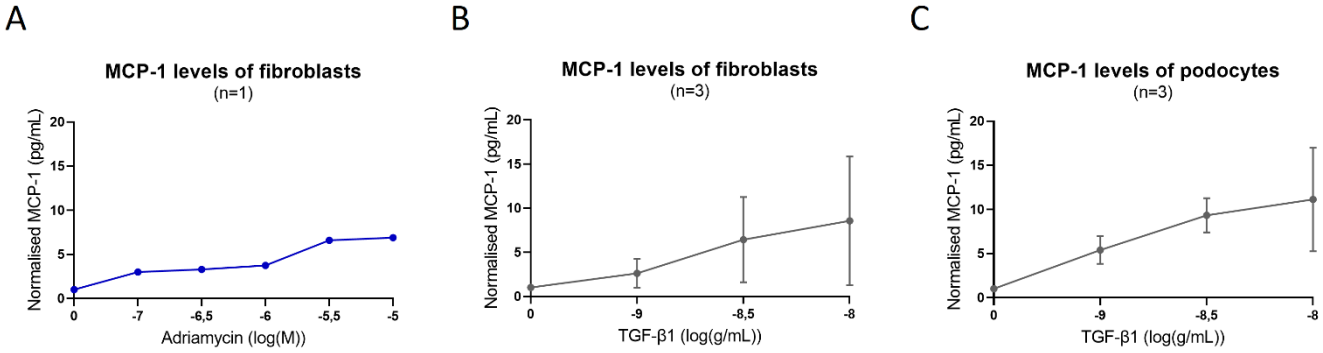

Figure 8: MCP-1 secretion levels measured in fibroblasts and podocytes via sandwich ELISA. **A|** MCP-1 quantitation in fibroblasts treated with Adriamycin. **B|** MCP-1 quantitation in fibroblasts treated with increasing concentrations of TGF-β1 with and without ALK-5 inhibitor. **C|** MCP-1 quantitation in podocytes treated with increasing concentrations of TGF-β1 with and without ALK-5 inhibitor. Statistical analysis by One-Way ANOVA (B and C). Errors bars showing standard deviation. n = 1 (**A**) and n = 3 (**B**, **C**).

MCP-1 levels associated with fibrotic ECM marker expression. To investigate possible relationships between MCP-1 secretion and ECM deposition markers, correlation analyses were performed in which MCP-1 levels were plotted against ECM protein marker expressions of collagen I, collagen IV, and fibronectin. Correlation analyses resulted in interesting findings. Whereas MCP-1 levels and ECM protein markers showed a non-linear relationship in fibroblasts (**Figure 9A-C**), a significant linear correlation was found between these two variables in podocytes (**Figure 9D-F**). These findings suggest an involvement of MCP-1 secretion in the deposition of pro-fibrotic ECM components.

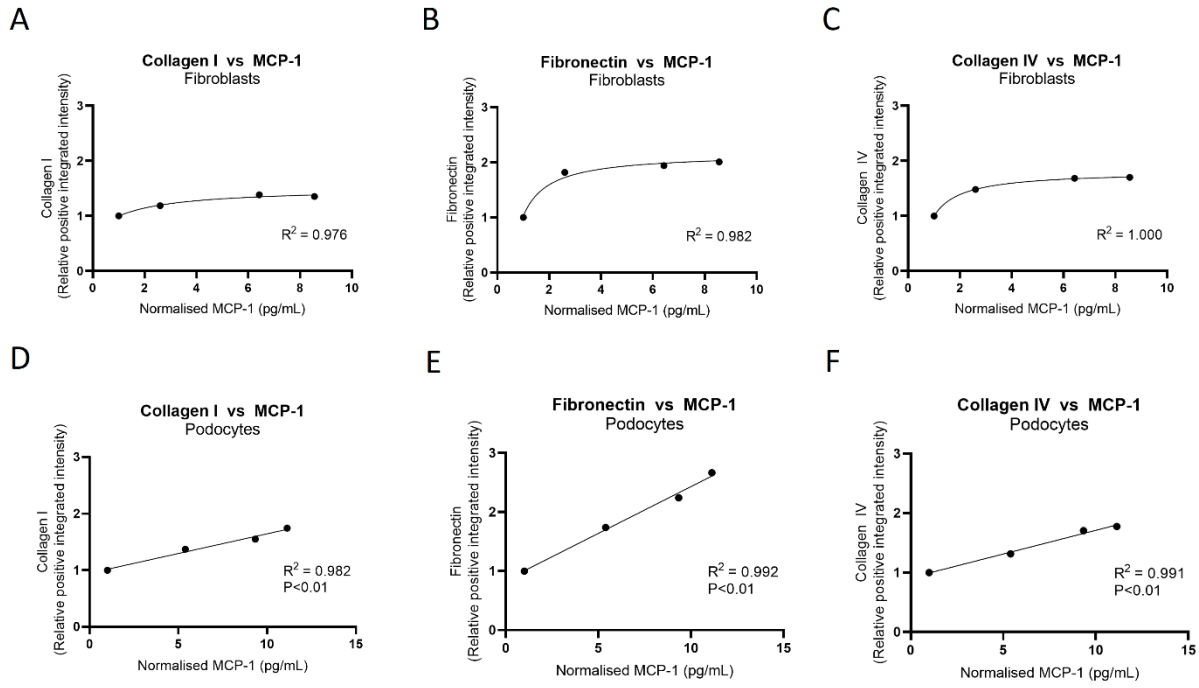

Figure 9: Correlation between MCP-1 levels and ECM biomarker expression. **A, B, C|** Non-linear association between the relative positive integrated intensity of different ECM markers and normalised MCP-1 levels in fibroblasts. High R^2 values were shown for collagen I (R^2 = 0.976), fibronectin (R^2 = 0.982), and collagen IV (R^2 = 1.000). **D, E, F|** Linear association between the relative positive integrated intensity of different ECM markers and normalised MCP-1 levels in podocytes. Significant R^2 values were shown for collagen I (R^2 = 0.982; P<0,01), fibronectin (R^2 = 0.992; P<0.01), and collagen IV (R^2 = 0.991; P<0.01). Statistical analysis by non-linear regression (**A-C**) and Pearson's correlation (**D-F**). n = 3.

ALK-5 inhibitor attenuates TGF-β1-induced fibrotic effects. To reverse the TGF-β1-induced fibrotic effects, primary cells were treated with pro-fibrotic markers in absence and presence of different drug compounds that appeared to have a fibrogenic inhibitory effect in literature. The ALK-5 inhibitor, SB431542, was able to significantly decrease the expression of the pro-fibrotic markers collagen I, collagen IV, and fibronectin upon TGF-β1 treatment as compared to the control in fibroblasts (**Figure 10**). The lack of inhibitory activity on αSMA can be explained by the absent significant increase upon TGF-β1 treatment (**Figure 5D**). Interestingly, the large error bars present in the control line graph (grey) disappear when cells were incubated with the ALK-5 inhibitor. This observation might suggest a drug activity irrelative from donor variation. Similar outcomes were shown in podocytes (**Figure 10**).

Whereas the ALK-5 inhibitor showed inhibitory effects in fibroblasts and podocytes, Pirfenidone did not result in decreasing pro-fibrotic biomarkers expression neither did the drug compound Nintedanib. Despite being unexpected, it is noteworthy that Nintedanib significantly decreases the protein expression of collagen IV when treated with 10 μM TGF-β1 in fibroblasts. The findings are detailed in the supplementary (**Supplementary figure 7-9**).

The ALK-5 inhibitor did not only reduce the protein expression of fibrotic biomarkers, but it also markedly reduced MCP-1 secretion to control levels in both fibroblasts and podocytes when treated with the highest concentrations of TGF-β1. Similar to the pro-fibrotic marker expression data, larger error bars disappeared when renal cells were treated with increasing TGF-β1 concentrations in presence of the ALK-5 inhibitor (**Figure 122**).

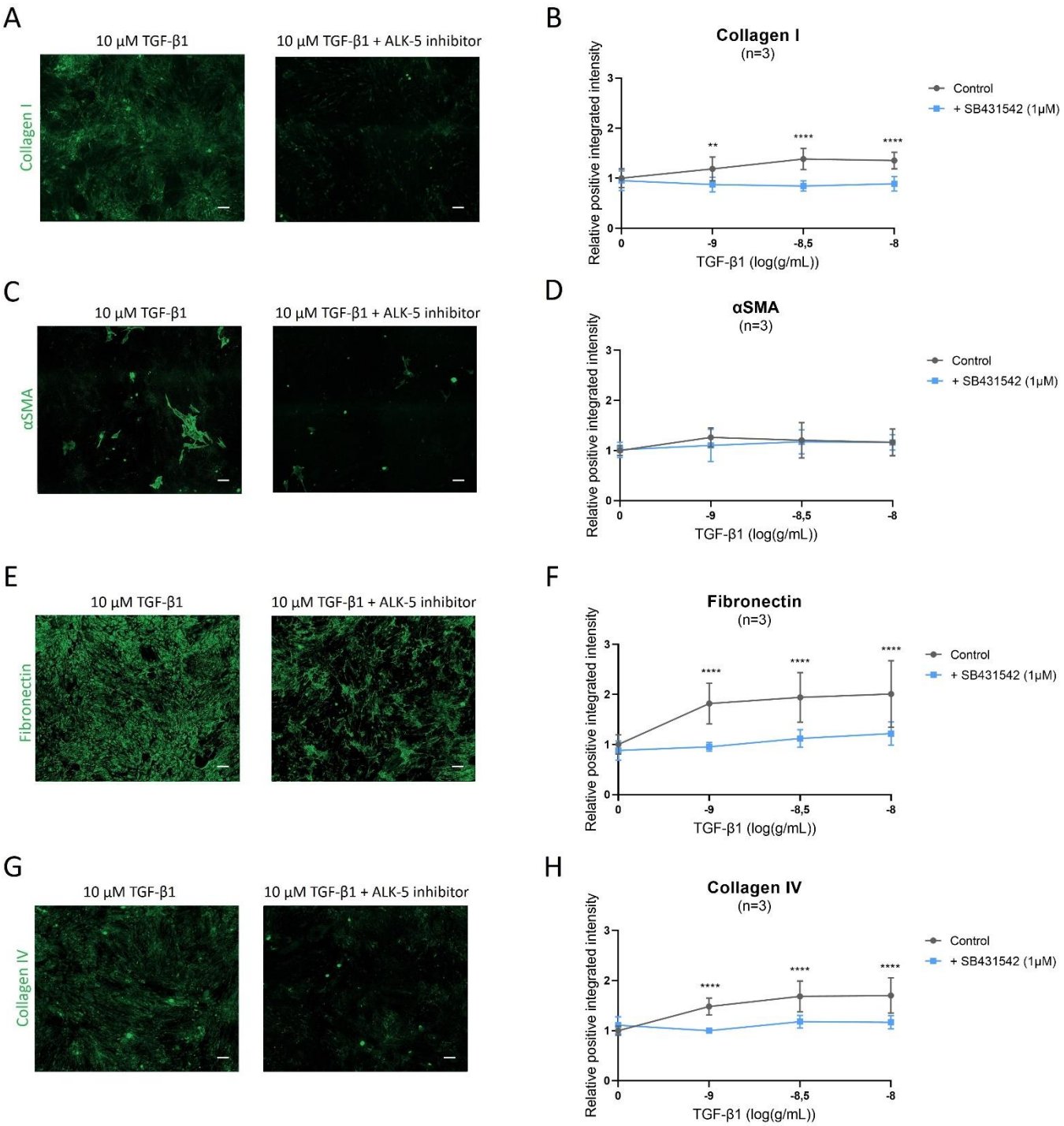

Figure 10: The histological effects of TGF-β1 and ALK-5 inhibitor treatment in human fibroblasts. **A, C, E, G|** Immunofluorescence with antibodies against, collagen I, αSMA, fibronectin, and collagen IV, respectively. Protein expression of the respective biomarkers were decreased when treated with 10 µM TGF-β1 + ALK-5 inhibitor (SB431542; 1 µM) as compared to treatment with 10 µM TGF-β1, with the exception of αSMA. **B, D, F, H|** Image intensity analysis for collagen I, αSMA, fibronectin, and collagen IV treated with increasing concentrations of TGF-β1 with and without ALK-5 inhibitor (SB431542; 1 µM). Results are expressed as relative positive integrated intensity. Statistical analysis by Two-Way ANOVA (B, D, F, and H), *P<0.05, ***P<0.001, ****P<000.1. Errors bars showing standard deviation. n = 3. The scalebar is 135 µm.

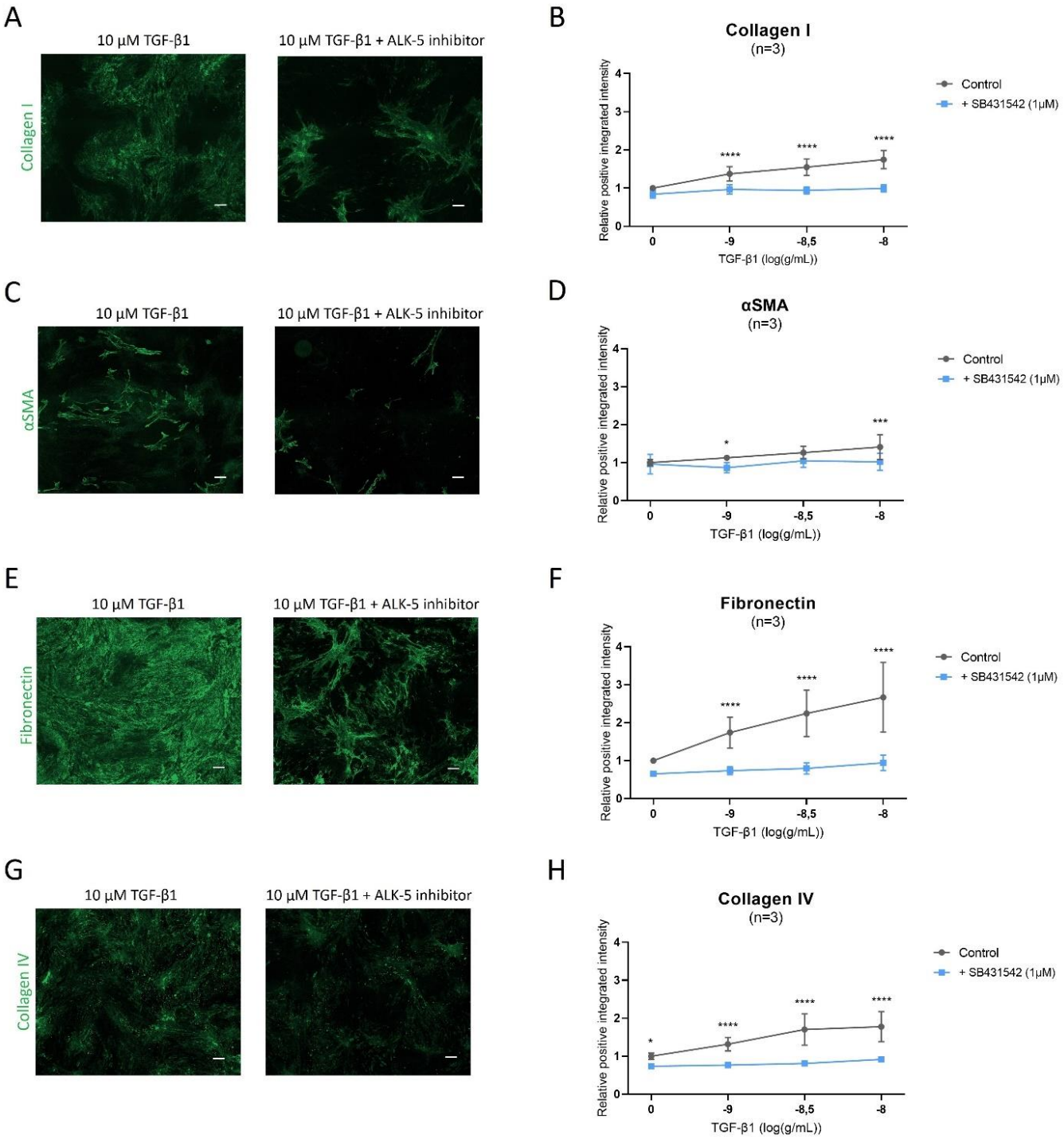

Figure 11: The histological effects of TGF-β1 and ALK-5 inhibitor treatment in human podocytes. **A, C, E, G|** Immunofluorescence with antibodies against, collagen I, αSMA, fibronectin, and collagen IV, respectively. Protein expression of the respective biomarkers were decreased when treated with 10 µM TGF-β1 + ALK-5 inhibitor (SB431542; 1 µM) as compared to treatment with 10 µM TGF-β1. **B, D, F, H|** Image intensity analysis for collagen I, αSMA, fibronectin, and collagen IV treated with increasing concentrations of TGF-β1 with and without ALK-5 inhibitor (SB431542; 1 µM). Results are expressed as relative positive integrated intensity. Statistical analysis by Two-Way ANOVA (B, D, F, and H), *P<0.05, ***P<0.001, ****P<000.1. Errors bars showing standard deviation. n = 3. The scalebar is 135 µm.

A

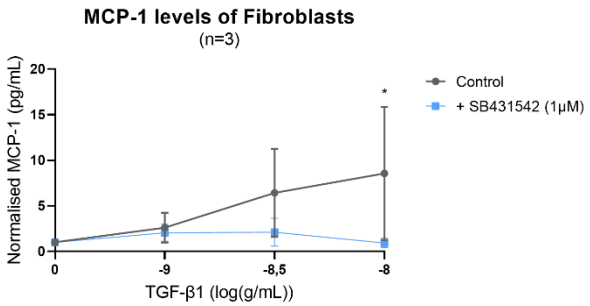

B

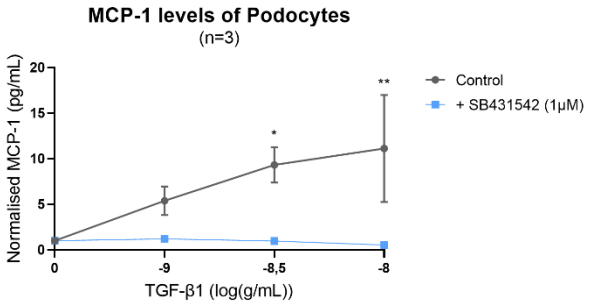

Figure 12: Inhibitory effect of SB431542 on MCP-1 secretion in human renal cells. **A|** Quantitation of MCP-1 levels in fibroblasts with increasing TGF-β1 concentrations in presence and absence of ALK-5 inhibitor (SB431542; 1 µM). Treatment with inhibitor showed significant decrease of MCP-1 levels. **B|** Quantitation of MCP-1 levels in podocytes with increasing TGF-β1 concentrations in presence and absence of ALK-5 inhibitor (SB431542; 1 µM). Treatment with inhibitor showed significant decrease of MCP-1 levels. Statistical analysis by Two-Way ANOVA (A and B), *P<0.05, **P<0.01. Errors bars showing standard deviation. n = 3.

Discussion

Chronic kidney disease, defined by a progressive loss of kidney function, poses a serious risk to human health accounting for a large burden worldwide. Renal fibrosis, the final manifestation of CKD, is the progressive maladaptive repair of kidney tissue injury which ultimately can lead to end-stage kidney failure. Despite the severity of this long-term progressive condition, the pathogenesis and effective treatment options of renal fibrosis remain to be elucidated.

Here, this study aimed to answer a part of this by developing an *in vitro* disease model for renal fibrosis of the glomerulus using human primary kidney cells. The outcomes of this study were used to answer the following research questions: 'To what extent is the developed kidney MPS disease model able to mimic the physiological environment of renal fibrosis? And to what extent can the fibrotic effects of this disease model be reversed?'. In this study, it has been hypothesised that treating the human kidney cells with fibrotic inducers might exert the presence of relevant pro-fibrotic biomarkers, hence physiological recapitulating renal fibrosis. Whereas treating the human kidney cells with fibrotic inhibitors, the induced expression of relevant pro-fibrotic markers can be reversed.

The validation experiments, performed prior to this study, demonstrate that the established isolation method successfully obtains fibroblasts and podocytes from human kidney cortexes. The isolation of the correct kidney cell types, using a well-validated isolation method, is of great importance in the development of a renal fibrosis model. It namely lowers the risk of a renal fibrotic MPS model reflecting interactions and cross talk between incorrect renal cell types. Moreover, it is crucial to accurately model renal fibrosis and predict the anti-fibrotic effects of drug compounds used in this study.

One of the conclusions that can be drawn from the experiments with the fibrogenic inducers is that the results obtained from this study are not entirely in line with literature and previous studies. An attempt was made to create a positive control for the renal fibrosis model by using the nephrotoxic compounds Adriamycin. Despite the fact that previous studies were able to develop an Adriamycin-induced nephropathy model in rodents, this study was not able to gather convincing evidence to substantiate the role of Adriamycin as a positive control for the cellular *in vitro* fibrosis model (Nogueira et al., 2017). Therefore, efforts should be made to investigate other nephrotoxic compounds that have the potential to be a suitable and reliable positive control in renal cells. A suggestion for a positive control could be cyclosporine A which has the potential to induce *in vitro* renal fibrosis as demonstrated by Slattery et al. (2005).

Whereas TGF-β1 was able to significantly increase the hallmark of renal fibrosis, no significant impact on the ECM deposition and myofibroblasts differentiation by AngII and TNFα treatments were observed in this study. The lack of an observable pro-fibrotic effect of TNFα and AngII is counterintuitive and inconsistent with previous studies reporting their contribution to the development of renal fibrosis. For instance, Therrien et al. (2012) demonstrated that neutralization of TNFα in rats with renal failure reduces the progression of renal fibrosis, hence showing evidence of a pro-fibrotic role of TNFα. Similarly, AngII has been demonstrated to increase the ECM deposition and negatively impact renal fibrosis in numerous studies (Faulkner et al., 2005; Y. Sun et al., 2000).

The discrepancy between the results from this study and previous studies may suggest that TNFα and AngII require a different experimental design, including longer treatment durations and/or different concentrations. Future research could therefore consider to reassess the experimental design and repeat the experiment in both fibroblasts and podocytes. Another explanation for the lack of fibrogenic effects is that these factors are involved in more complex and/or systemic biological processes which are not recapitulated by the fibrosis model in this study. Therefore, simply incubating primary cells with these factors does not result in the desired fibrotic effects.

TGF-β1 treatment did not only affect the protein expression of fibrotic markers and MCP-1 secretion, but also resulted alterations in cellular morphology of both renal cell types. The fibroblasts and podocytes in this study were observed with nuclear and cellular hypertrophy which may demonstrate indications of cellular stress response. Cellular stress is known to occur as a response to different stimuli, including tissue injury and inflammation (Miller & Zachary, 2017). The findings of this study are in accordance with existing literature describing the cellular stress response in podocytes, however, no hypertrophic alterations have been identified in fibroblasts (Kriz et al., 2013). Therefore, to the best of my knowledge, this study is the first to demonstrate hypertrophic response in renal fibroblasts as a response to TGF-β1 treatment. The hypertrophic response to TGF-β1 treatment also substantiates the ongoing debate about whether this cytokine is directly linked to renal hypertrophy, particularly impacting renal tubular epithelial cells and podocytes (Sharma & Ziyadeh, 1994; Yu et al., 2019).

An interesting correlation observed in this study is between MCP-1 secretion and the production of ECM protein markers. Interestingly, a study performed by Park et al., (2008) demonstrates that inhibition of the MCP-1/C-C chemokine receptor type 2 (CCR2) system significantly reduced the TGF-β1-induced ECM marker expression. The association observed in this study is therefore consistent with literature stating that MCP-1 is not only involved in the recruitment of leukocytes, but also seems

to play a role in the progression of renal fibrosis by mediating the ECM deposition in both fibroblasts and podocytes (Eun et al., 2009a; Giunti et al., 2008; Schneider et al., 1999).

The selection of drug compounds used in this study to attenuate the induced pro-fibrotic effects were based on previously published data that showed therapeutic effects. The ALK-5 inhibitor, SB431542, was able to significantly inhibit the MCP-1 secretion as well as the protein expression of almost all fibrotic markers in fibroblasts and podocytes. Its most striking inhibitory effect is on the deposition of fibronectin, accounting for a 40% decrease in expression compared to the control. These findings successfully support the data shown by Eun et al. (2009b) demonstrating the inhibitory effect of the drug on MCP-1 levels in podocytes. The activity of the ALK-5 inhibitor is not surprising considering the mode of action of the drug compound, namely suppressing the most prominent receptors in the development of renal fibrosis: the TGF-β type I receptor/ALK-5 (Inman et al., 2002). This inhibitor might be a potential new treatment against renal fibrosis.

Contrary to the expectations, the collated data did not show evidence for Pirfenidone and Nintedanib decreasing the protein expression of the pro-fibrotic markers. Both anti-fibrotic compounds are FDA-approved treatments against idiopathic pulmonary fibrosis (IPF) (Hadda & Guleria, 2020). Whereas Pirfenidone is proposed to attenuates fibrotic effects by targeting the TNF pathways, platelet activation, and cellular oxidation, Nintedanib supresses tyrosine kinase receptors of various growth factor receptors (e.g., fibroblast-, platelet-derived, and vascular receptors) (Aravena et al., 2015; Wollin et al., 2015). Besides their effectiveness in IPF, Pirfenidone and Nintedanib also appeared to be effective in attenuation of renal fibrosis in rodents, respectively, as demonstrated by Hewitson et al. (2001) and (Hadda & Guleria, 2020). The lack of anti-fibrotic activity shown in this study is surprising and therefore not in line with previous studies.

The inconsistency could possibly be explained by the lack of metabolic activity due to the *in vitro* feature of this fibrotic model. In contrast to SB431542, Pirfenidone and Nintedanib are namely known to undergo bioactivation mediated by CYP1A2 enzyme and esterases, respectively (Wind et al., 2019; Zhou et al., 2020). The chemical structure of Pirfenidone used in this study, for instances, differs from the structure of the biological active metabolite. It namely lacks a carboxyl group which might negatively impact the binding to its target and therefore explains the lack of anti-fibrotic effect shown in this study (N. Sun et al., 2016).

While this study successfully developed *in vitro* renal fibrosis using TGF-β1 and identified a potential anti-renal fibrosis treatment, several limitations might have influenced the experimental data naturally. One of them is the lack of donor eligibility criteria. The implementation of clearly defined donor eligibility criteria might reduce the high donor variation shown in this study. The high variation

is represented by the large error bars and most likely caused by donor-specific responses to fibrogenic treatments. By defining criteria, such as age, medical history, genetic diseases, and substance usage, the inter-donor variation could be reduced and might lead to more consistent and generalizable outcomes. Further research that takes these variable into account needs to be carried out.

Due to time constraints, not all pro-fibrotic treatments and/or drug compounds were performed in three biological repeats or in both kidney cell types (e.g., Adriamycin, AngII, TNFα, and Nintedanib). Besides, the obtained results are based on a relatively small donor population (n=3). One could argue that the significant results obtained from this study might even be non-significant when increasing the amount of biological repeats. Or, vice versa, that significant results might be even more significant when performed in more biological repeats. Therefore, conclusions should be made and interpreted with caution and future research should consider a higher number of biological repeats to reduce the uncertainty of potential unreliable results.

Apart from replicating the study in a larger kidney donor population and implementing clear donor eligibility criteria, a suggestion for future research would be the development of a multi-cellular renal fibrosis model. This multi-cellular model has the potential to more accurately recapitulate the interplay between different renal cell types involved in this disease. Moreover, a multi-cellular model can be developed to mimic the different hallmarks of renal fibrosis. Glomerulosclerosis could for instance be mimicked by developing a multi-cellular model using endothelial cells, fibroblasts, and podocytes. Tubulointerstitial fibrosis, on the other hand, can be recapitulated with the use of PTCs and podocytes.

Conclusion

The purpose of this study was to develop an *in vitro* renal fibrosis model. Recapitulating the fibrotic effects of the glomerulus using human primary kidney cells and reversing these effects was the main focus of this study. The most important outcomes from the development of the *in vitro* model are the following: 1) TGF-β1 was identified as a potent fibrotic driver; 2) human primary kidneys cells show characteristics of cellular stress under fibrotic circumstances; 3) the cytokine MCP-1 shows strong indications of ECM deposition involvement; and 4) the ALK-5 inhibitor can be considered as a potent renal anti-fibrotic agent.

The findings successfully answers the research question which partly confirms the hypothesis, namely that by treating human renal primary cells with fibrogenic inducers and fibrogenic inhibitors *in vitro* renal fibrosis can be developed and reversed, respectively. The acquired knowledge and developed disease model open up new avenues for the understanding of the pathogenesis underlying renal fibrosis. Furthermore, this renal fibrotic model makes an important first step towards a standardised and reproducible commercial model that has the great potential to aid in the drug discovery of anti-fibrotic therapies and reduce the worrying risk of CKD.

Supplementary

Figure S1

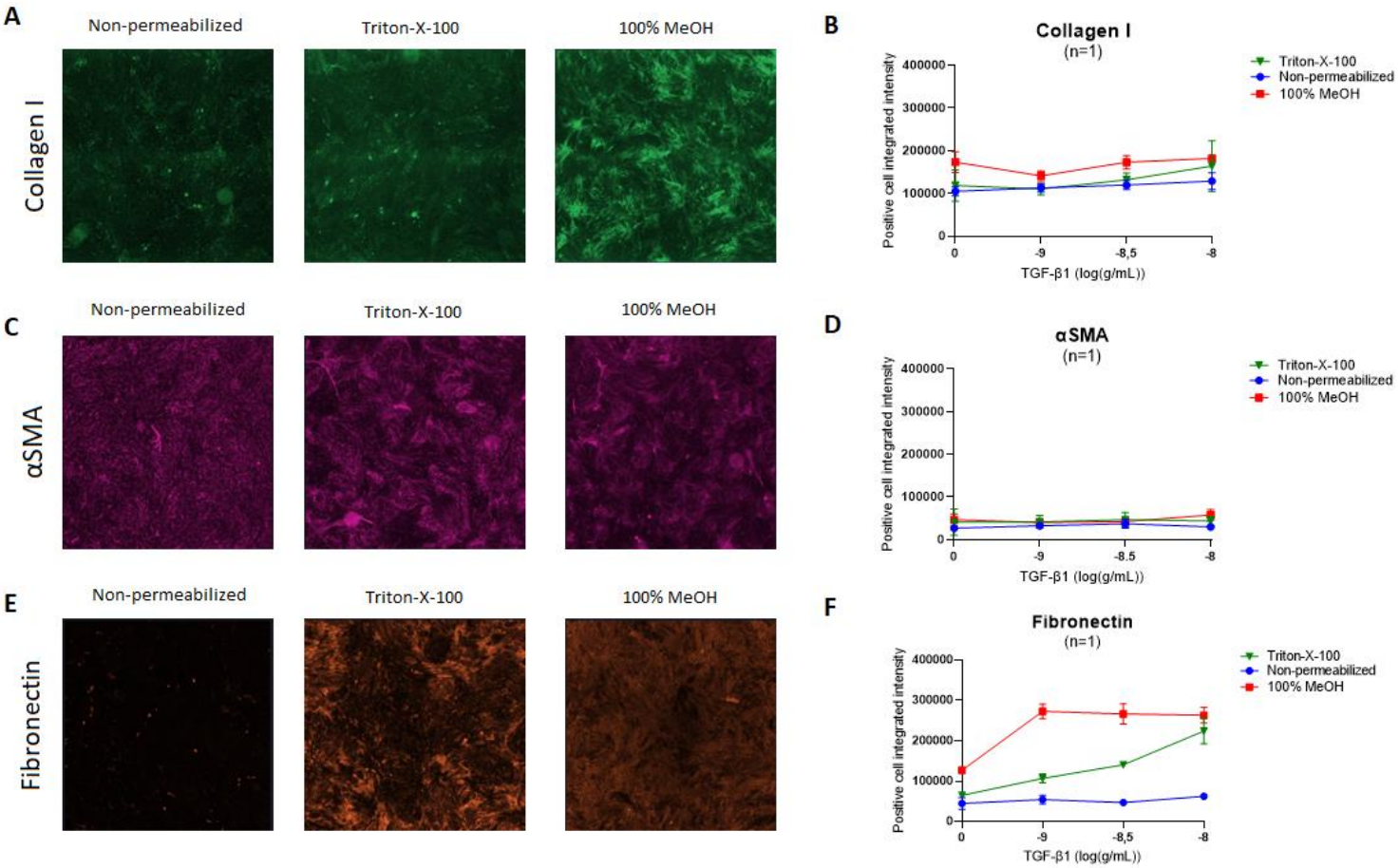

Supplementary figure 1: Immunofluorescence permeabilization optimisation in human fibroblasts. **A, C, E|** Immunofluorescence staining with antibodies against collagen I, αSMA, and fibronectin without permeabilization (left), permeabilization with Trition-X-100 (middle), and permeabilization with 100% methanol (right; MeOH). **B, D, F|** Image intensity analysis for collagen I, αSMA, and fibronectin permeabilized with different methods after treated with increasing concentrations of TGF-β1. Results are expressed as positive cell integrated intensity. Errors bars showing standard deviation. n = 1.

Figure S2

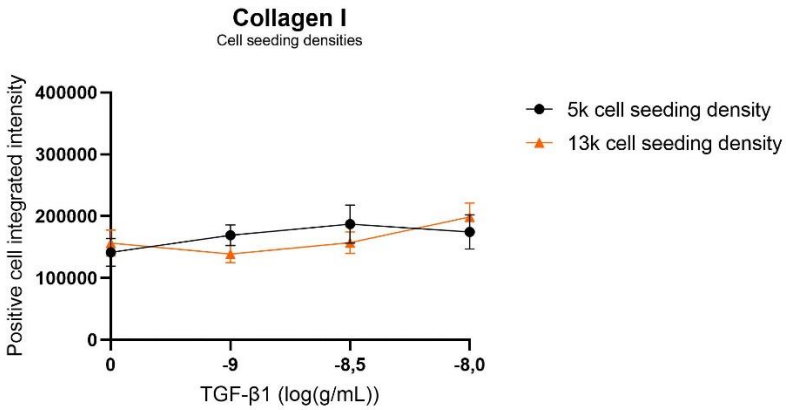

Supplementary figure 2: Cell seeding density optimisation in human podocytes. Immunofluorescence staining of collagen I in TGF-β1-treated podocytes seeded out with a cell density of 5k (black line) and 13k (orange line). Results are expressed as positive cell integrated intensity. Errors bars showing standard deviation. n = 1.

Figure S3

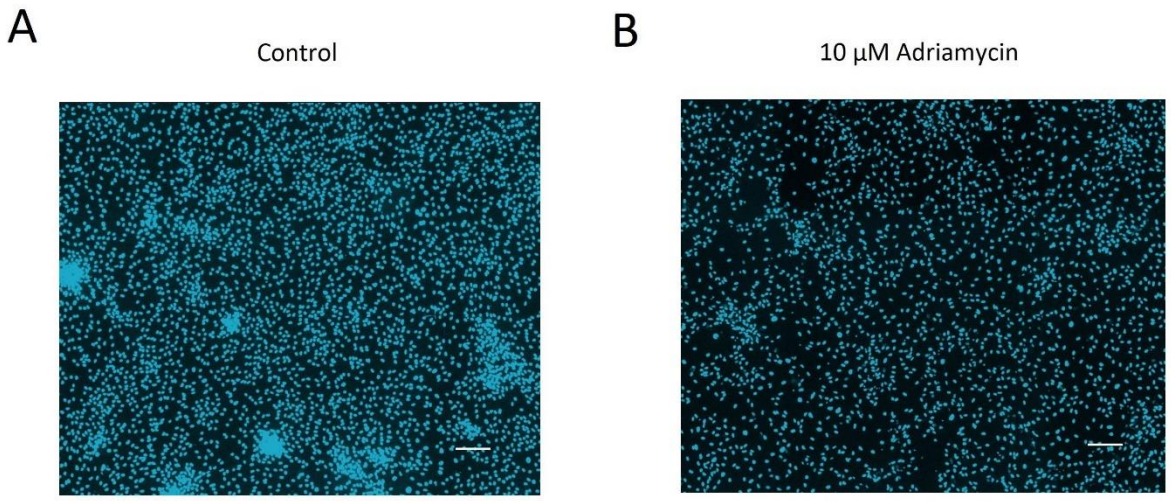

Supplementary figure 3: The effect of Adriamycin on fibroblast viability. **A|** Control fibroblasts stained for DAPI indicative for the amount of nuclei present in the cell culture when treated without Adriamycin (Control). **B|** Fibroblasts stained for DAPI indicative for the amount of nuclei present in the cell culture when treated with the highest concentration of Adriamycin (10 µM). The highest concentration of Adriamycin reduces the amount of nuclei in the cell culture when compared to the control (**A**). The scalebar is 135 µm.

Figure S4

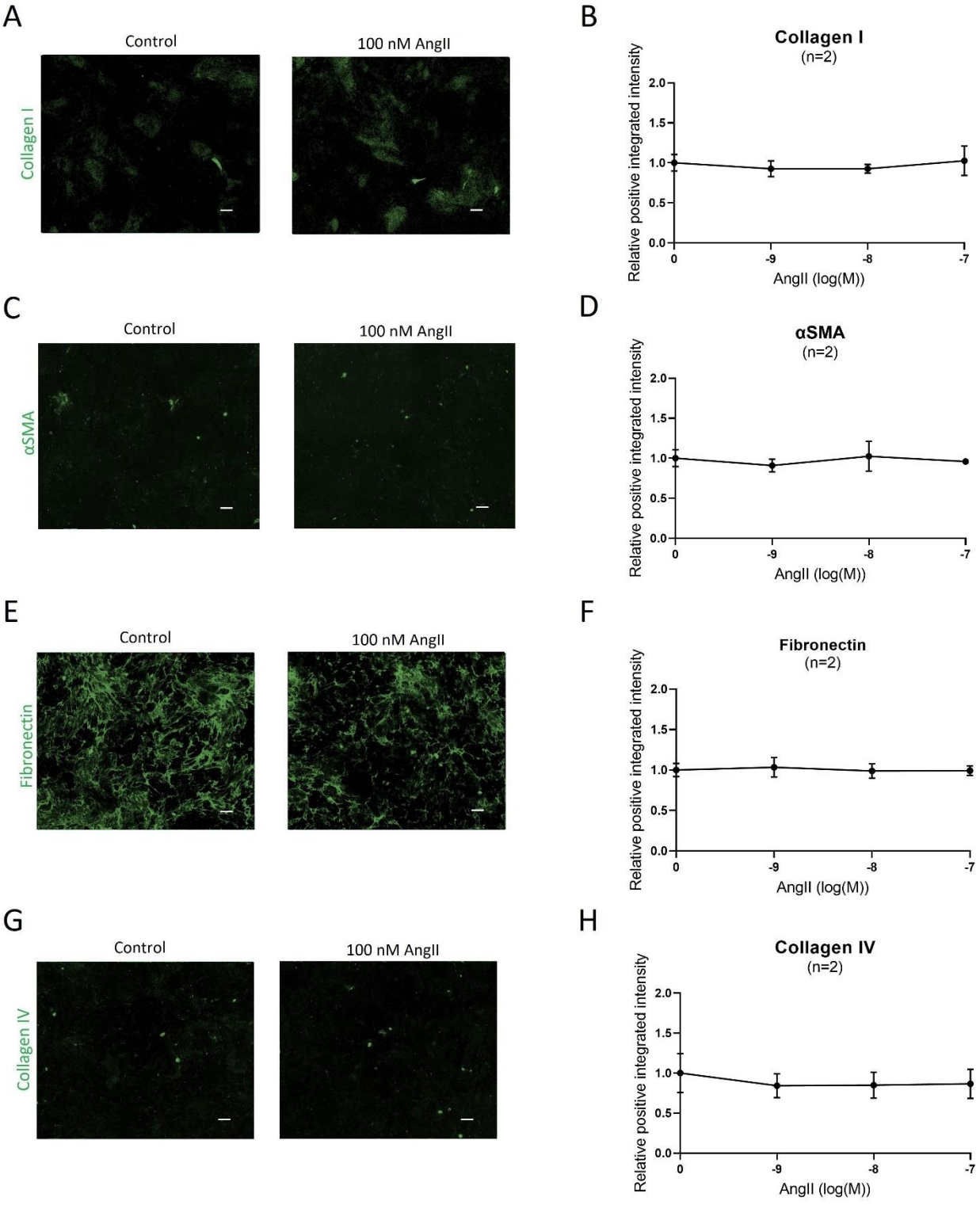

Supplementary figure 4: The histological effects of AngII treatment in human fibroblasts. **A, C, E, G|** Immunofluorescence with antibodies against, collagen I, αSMA, fibronectin, and collagen IV, respectively. Protein expression of the respective biomarkers were not significantly changed when treated with 100 nM AngII as compared to the control. **B, D, F, H|** Image intensity analysis for collagen I, αSMA, fibronectin, and collagen IV treated with increasing concentrations of AngII. Results are expressed as relative positive integrated intensity. Statistical analysis by One-Way ANOVA (B, D, F, and H). Errors bars showing standard deviation. n = 2. The scalebar is 135 µm

Figure S5

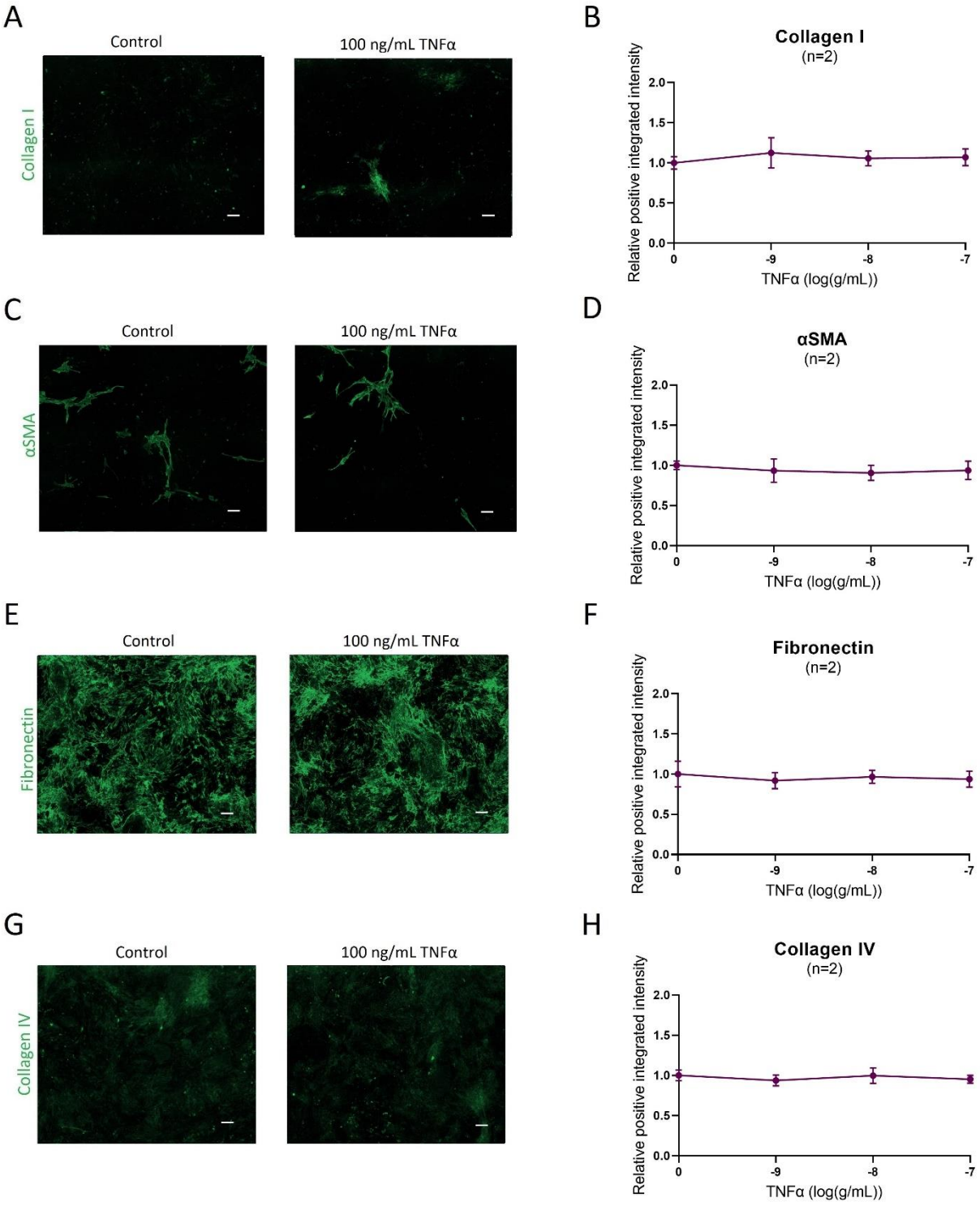

Supplementary figure 5: The histological effects of TNFα treatment in human fibroblasts. **A, C, E, G|** Immunofluorescence with antibodies against, collagen I, αSMA, fibronectin, and collagen IV, respectively. Protein expression of the respective biomarkers were not significantly changed when treated with 100 ng/mL TNFα as compared to the control. **B, D, F, H|** Image intensity analysis for collagen I, αSMA, fibronectin, and collagen IV treated with increasing concentrations of TNFα. Results are expressed as relative positive integrated intensity. Statistical analysis by One-Way ANOVA (B, D, F, and H). Errors bars showing standard deviation. n = 2. The scalebar is 135 µm.

Figure S6

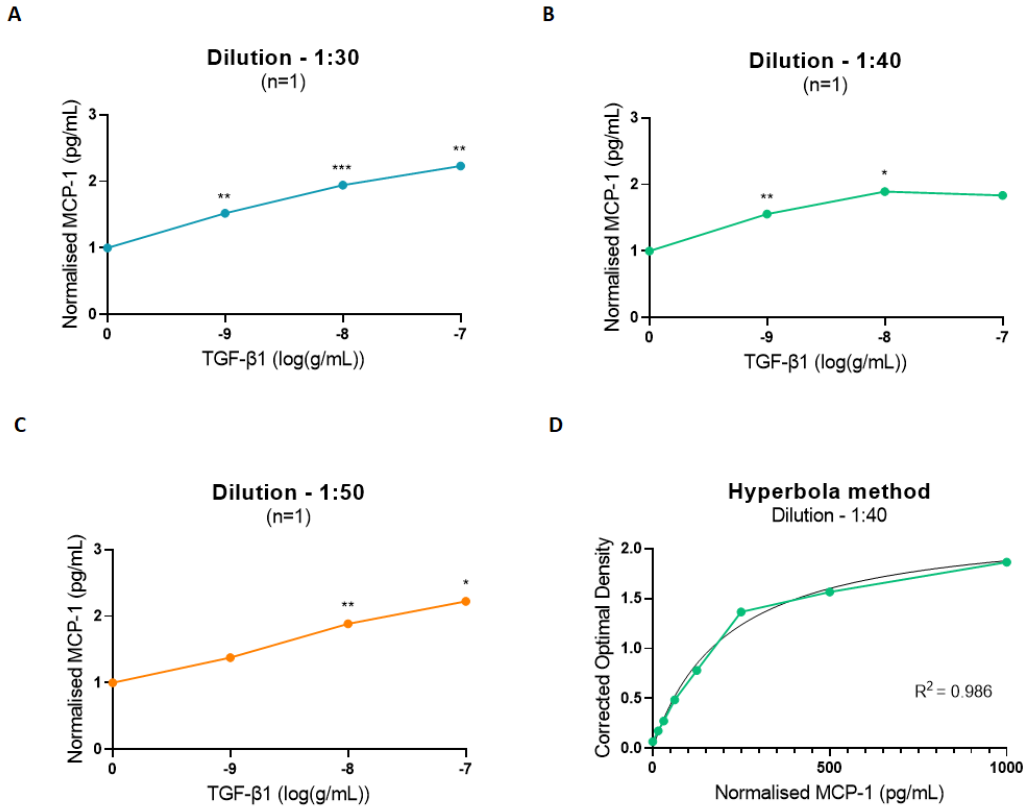

Supplementary figure 6: Sandwich ELISA sample dilution optimisation of MCP-1 in human fibroblasts. A, B, C| Quantitation of MCP-1 levels in fibroblasts treated with increasing TGF-β1 concentrations using 30x (**A**), 40x (**B**), and 50x (**C**) sample dilutions. **D|** Correlation analysis between the corrected optimal density and normalised MCP-1 levels using the optimal ELISA sample dilution factor (1:40) resulting in a R^2 of 0.986. Statistical analysis by One-Way ANOVA (**A**-**C**) and hyperbolic regression (**D**), *P<0.05, **P<0.01, ***P<0.001. n = 1.

Figure S7

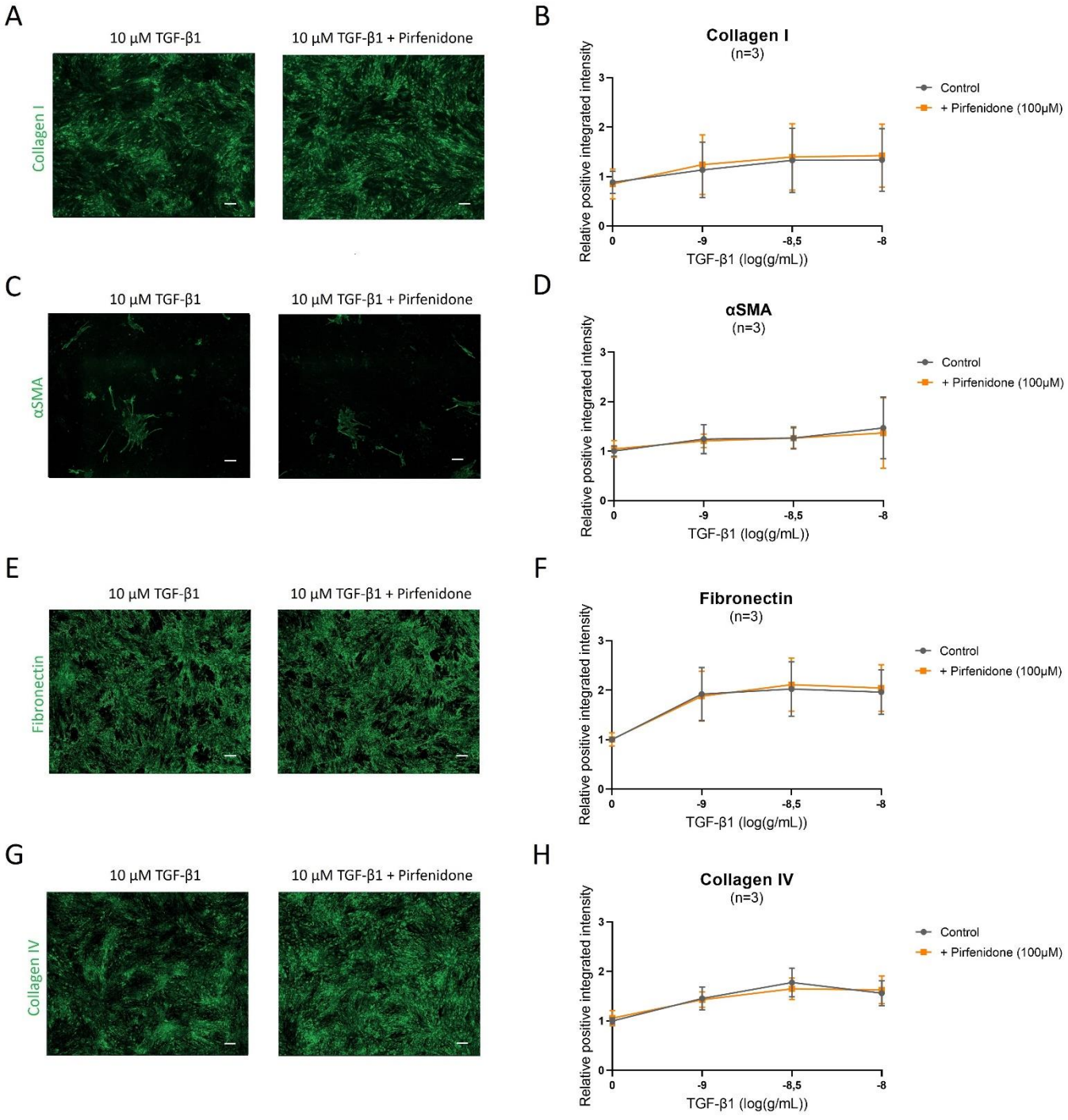

Supplementary figure 7: The histological effects of TGF-β1 and Pirfenidone treatment in human fibroblasts. **A, C, E, G|** Immunofluorescence with antibodies against, collagen I, αSMA, fibronectin, and collagen IV, respectively. Protein expression of the respective biomarkers were not decreased when treated with 10 µM TGF-β1 + 100 µM Pirfenidone as compared to treatment with 10 µM TGF-β1. **B, D, F, H|** Image intensity analysis for collagen I, αSMA, fibronectin, and collagen IV treated with increasing concentrations of TGF-β1 with and without 100 µM Pirfenidone. Results are expressed as relative positive integrated intensity. Statistical analysis by Two-Way ANOVA (**B**, **D**, **F**, and **H**). Errors bars showing standard deviation. n = 3. The scalebar is 135 µm.

Figure S8

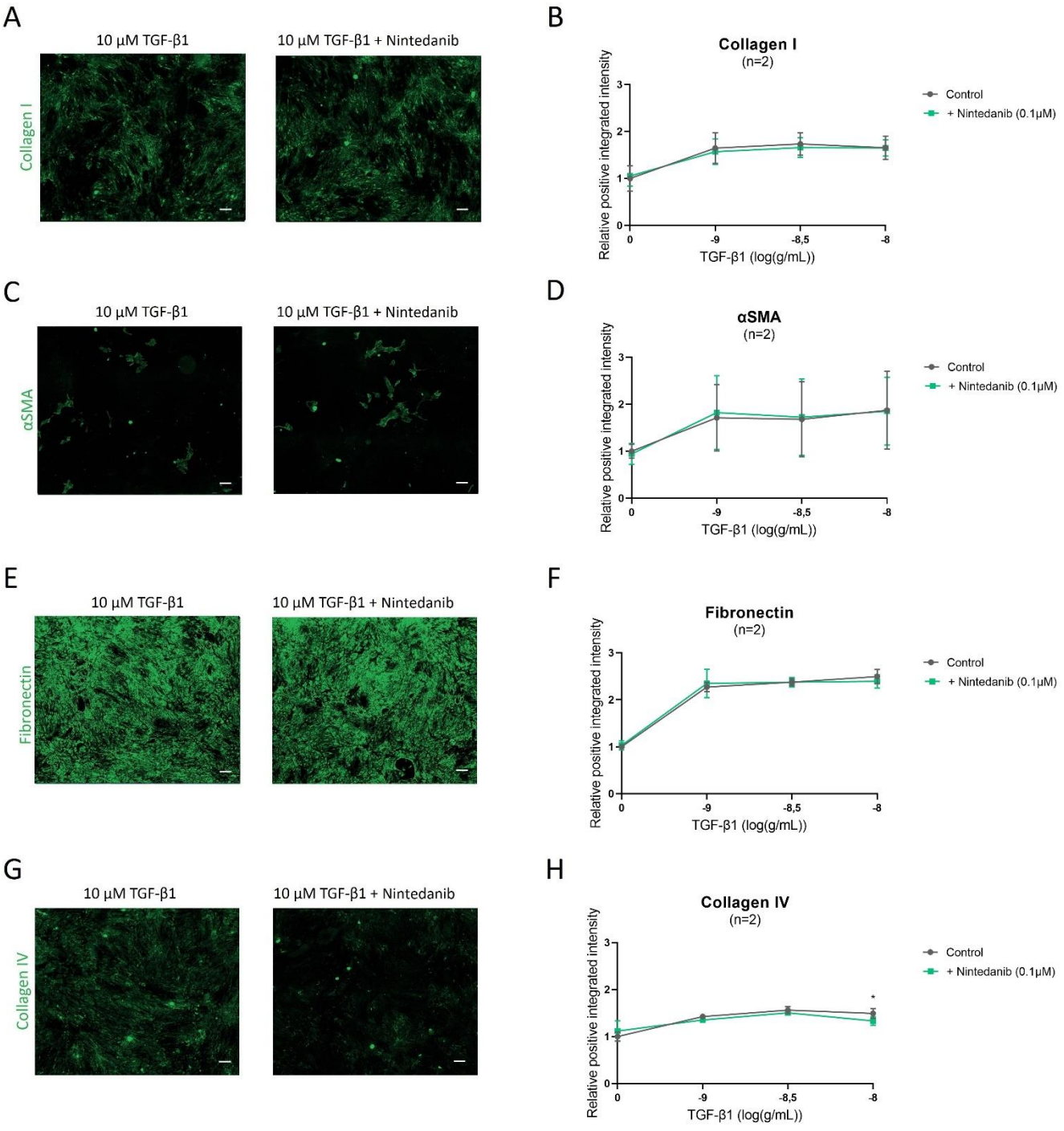

Supplementary figure 8: The histological effects of TGF-β1 and Nintedanib treatment in human fibroblasts. **A, C, E, G|** Immunofluorescence with antibodies against, collagen I, αSMA, fibronectin, and collagen IV, respectively. Protein expression of the respective biomarkers were not decreased when treated with 10 µM TGF-β1 + 0.1 µM Nintedanib as compared to treatment with 10 µM TGF-β1. **B, D, F, H|** Image intensity analysis for collagen I, αSMA, fibronectin, and collagen IV treated with increasing concentrations of TGF-β1 with and without 0.1 µM Nintedanib. Results are expressed as relative positive integrated intensity. Statistical analysis by Two-Way ANOVA (**B**, **D**, **F**, and **H**), *P<0.05. Errors bars showing standard deviation. n = 2. The scalebar is 135 µm.

Figure S9

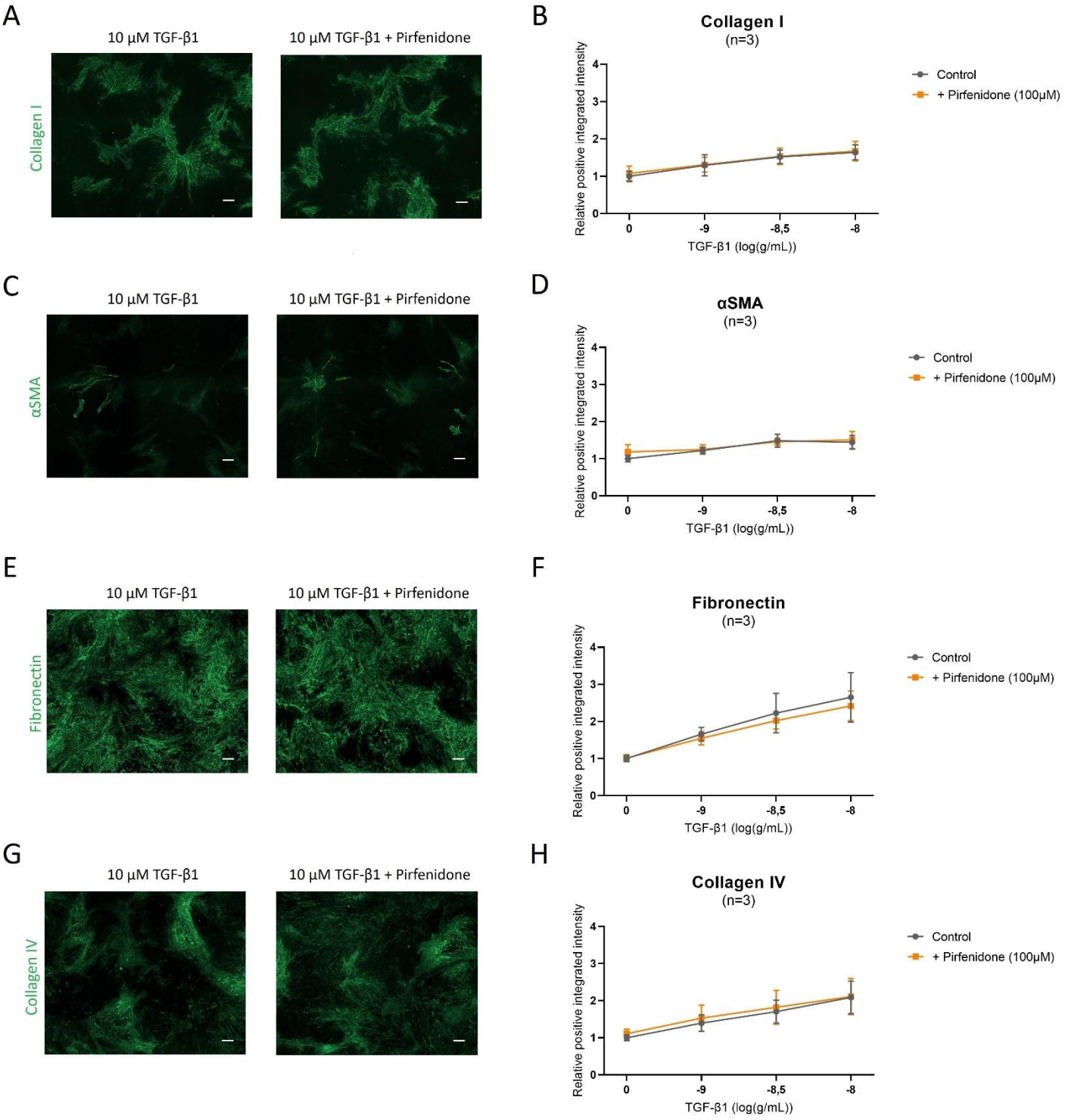

Supplementary Figure 9: The histological effects of TGF-β1 and Pirfenidone treatment in human podocytes. **A, C, E, G|** Immunofluorescence with antibodies against, collagen I, αSMA, fibronectin, and collagen IV, respectively. Protein expression of the respective biomarkers were not decreased when treated with 10 µM TGF-β1 + 100 µM Pirfenidone as compared to treatment with 10 µM TGF-β1. **B, D, F, H|** Image intensity analysis for collagen I, αSMA, fibronectin, and collagen IV treated with increasing concentrations of TGF-β1 with and without 100 µM Pirfenidone. Results are expressed as relative positive integrated intensity. Statistical analysis by Two-Way ANOVA (**B**, **D**, **F**, and **H**), *P<0.05. Errors bars showing standard deviation. n = 3. The scalebar is 135 µm.

References

Aravena, C., Labarca, G., Venegas, C., Arenas, A., & Rada, G. (2015). Pirfenidone for Idiopathic Pulmonary Fibrosis: A Systematic Review and Meta-Analysis. *PloS One*, *10*(8).

Bikbov, B., Purcell, C. A., Levey, A. S., Smith, M., Abdoli, A., Abebe, M., Adebayo, O. M., Afarideh, M., Agarwal, S. K., Agudelo-Botero, M., Ahmadian, E., Al-Aly, Z., Alipour, V., Almasi-Hashiani, A., Al-Raddadi, R. M., Alvis-Guzman, N., Amini, S., Andrei, T., Andrei, C. L., … Murray, C. J. L. (2020). Global, regional, and national burden of chronic kidney disease, 1990–2017: a systematic analysis for the Global Burden of Disease Study 2017. *The Lancet*, *395*(10225), 709–733.

Black, L. M., Lever, J. M., & Agarwal, A. (2019). Renal Inflammation and Fibrosis: A Double-edged Sword. *Journal of Histochemistry and Cytochemistry*, *67*(9), 663.

Borthwick, L. A., Wynn, T. A., & Fisher, A. J. (2013). Cytokine mediated tissue fibrosis. *Biochimica et Biophysica Acta (BBA) - Molecular Basis of Disease*, *1832*(7), 1049–1060.

Brown, C. D. A., Sayer, R., Windass, A. S., Haslam, I. S., de Broe, M. E., D'Haese, P. C., & Verhulst, A. (2008). Characterisation of human tubular cell monolayers as a model of proximal tubular xenobiotic handling. *Toxicology and Applied Pharmacology*, *233*(3), 428–438.

Bülow, R. D., & Boor, P. (2019). Extracellular Matrix in Kidney Fibrosis: More Than Just a Scaffold. In *Journal of Histochemistry and Cytochemistry* (Vol. 67, Issue 9, pp. 643–661). SAGE Publications Ltd.

Cañadas-Garre, M., Anderson, K., Cappa, R., Skelly, R., Smyth, L. J., McKnight, A. J., & Maxwell, A. P. (2019). Genetic susceptibility to chronic kidney disease - Some more pieces for the heritability puzzle. *Frontiers in Genetics*, *10*(MAY), 453.

Chen, W. Y., Evangelista, E. A., Yang, J., Kelly, E. J., & Yeung, C. K. (2021). Kidney Organoid and Microphysiological Kidney Chip Models to Accelerate Drug Development and Reduce Animal Testing. *Frontiers in Pharmacology*, *12*.

Eddy, A. A. (2011). The TGF-β Route to Renal Fibrosis Is Not Linear: The miR-21 Viaduct. *Journal of the American Society of Nephrology*, *22*(9), 1573–1575.

Efstratiadis, G., Divani, M., Katsioulis, E., & Vergoulas, G. (2009). Renal fibrosis. *Hippokratia*, *13*(4), 224.

Eun, Y. L., Choon, H. C., Khoury, C. C., Tet, K. Y., Pyagay, P. E., Wang, A., & Chen, S. (2009a). The monocyte chemoattractant protein-1/CCR2 loop, inducible by TGF-β, increases podocyte motility and albumin permeability. *American Journal of Physiology - Renal Physiology*, *297*(1), F85.

Eun, Y. L., Choon, H. C., Khoury, C. C., Tet, K. Y., Pyagay, P. E., Wang, A., & Chen, S. (2009b). The monocyte chemoattractant protein-1/CCR2 loop, inducible by TGF-β, increases podocyte motility and albumin permeability. *American Journal of Physiology - Renal Physiology*, *297*(1), F85.

Faulkner, J. L., Szcykalski, L. M., Springer, F., & Barnes, J. L. (2005). Origin of Interstitial Fibroblasts in an Accelerated Model of Angiotensin II-Induced Renal Fibrosis. *The American Journal of Pathology*, *167*(5), 1193–1205.

Giunti, S., Tesch, G. H., Pinach, S., Burt, D. J., Cooper, M. E., Cavallo-Perin, P., Camussi, G., & Gruden, G. (2008). Monocyte chemoattractant protein-1 has prosclerotic effects both in a mouse model of experimental diabetes and in vitro in human mesangial cells. *Diabetologia*, *51*(1), 198–207.

Guerrot, D., Dussaule, J. C., Kavvadas, P., Boffa, J. J., Chadjichristos, C. E., & Chatziantoniou, C. (2012). Progression of renal fibrosis: The underestimated role of endothelial alterations. *Fibrogenesis and Tissue Repair*, *5*(SUPPL.1), 1–6.

Hadda, V., & Guleria, R. (2020). Antifibrotic drugs for idiopathic pulmonary fibrosis: What we should know? *The Indian Journal of Medical Research*, *152*(3), 177.

Hewitson, T. D., Kelynack, K. J., Tait, M. G., Martic, M., Jones, C. L., Margolin, S. B., & Becker, G. J. (2001). Pirfenidone reduces in vitro rat renal fibroblast activation and mitogenesis. *Journal of Nephrology*, *14*(6), 453–460.

Inman, G. J., Nicolás, F. J., Callahan, J. F., Harling, J. D., Gaster, L. M., Reith, A. D., Laping, N. J., & Hill, C. S. (2002). SB-431542 is a potent and specific inhibitor of transforming growth factor-beta superfamily type I activin receptor-like kinase (ALK) receptors ALK4, ALK5, and ALK7. *Molecular Pharmacology*, *62*(1), 65–74.

Kovesdy, C. P. (2022). Epidemiology of chronic kidney disease: an update 2022. *Kidney International Supplements*, *12*(1), 7.

Kriz, W., Shirato, I., Nagata, M., LeHir, M., & Lemley, K. V. (2013). The podocyte's response to stress: The enigma of foot process effacement. *American Journal of Physiology - Renal Physiology*, *304*(4).

Liu, Y. (2006). Renal fibrosis: new insights into the pathogenesis and therapeutics. *Kidney International*, *69*(2), 213–217.

Liu, Y. (2011). Cellular and molecular mechanisms of renal fibrosis. *Nature Reviews. Nephrology*, *7*(12), 684.

Lv, W., Booz, G. W., Wang, Y., Fan, F., & Roman, R. J. (2018). Inflammation and renal fibrosis: recent developments on key signaling molecules as potential therapeutic targets. *European Journal of Pharmacology*, *820*, 65.

Mallappallil, M., Friedman, E. A., Delano, B. G., Mcfarlane, S. I., & Salifu, M. O. (2014). Chronic kidney disease in the elderly: evaluation and management. *Clinical Practice (London, England)*, *11*(5), 525.

Meng, X. M., Tang, P. M. K., Li, J., & Lan, H. Y. (2015). TGF-β/Smad signaling in renal fibrosis. *Frontiers in Physiology*, *6*(MAR), 82.

Mezzano, S. A., Ruiz-Ortega, M., & Egido, J. (2001). Angiotensin II and Renal Fibrosis. *Hypertension*, *38*(3 Pt 2), 635–638. https://doi.org/10.1161/HY09T1.094234

Miller, M. A., & Zachary, J. F. (2017). Mechanisms and Morphology of Cellular Injury, Adaptation, and Death. *Pathologic Basis of Veterinary Disease*, 2.

Murphy, A. M., Wong, A. L., & Bezuhly, M. (2015). Modulation of angiotensin II signaling in the prevention of fibrosis. In *Fibrogenesis and Tissue Repair* (Vol. 8, Issue 1). BioMed Central Ltd.

Ni, L., Saleem, M., & Mathieson, P. W. (2012). Podocyte culture: tricks of the trade. *Nephrology (Carlton, Vic.)*, *17*(6), 525–531.

Nogueira, A., Joao Pires, M., & Oliveira, P. (2017). Pathophysiological Mechanisms of Renal Fibrosis: A Review of Animal Models and Therapeutic Strategies. *In Vivo*, *31*(1), 1–22.

Panizo, S., Martínez-Arias, L., Alonso-Montes, C., Cannata, P., Martín-Carro, B., Fernández-Martín, J. L., Naves-Díaz, M., Carrillo-López, N., & Cannata-Andía, J. B. (2021). Fibrosis in chronic kidney disease: Pathogenesis and consequences. In *International Journal of Molecular Sciences* (Vol. 22, Issue 1, pp. 1–19). MDPI AG.

Park, J., Ryu, D. R., Li, J. J., Jung, D. S., Kwak, S. J., Lee, S. H., Yoo, T. H., Han, S. H., Lee, J. E., Kim, D. K., Moon, S. J., Kim, K., Han, D. S., & Kang, S. W. (2008). MCP-1/CCR2 system is involved in high glucose-induced fibronectin and type IV collagen expression in cultured mesangial cells. *American Journal of Physiology - Renal Physiology*, *295*(3), 749–757.

Pinto, S., Hoek, M., Huang, Y., Costet, P., Ma, L., & Imbriglio, J. E. (2017). Drug Discovery in Tissue Fibrosis. *Comprehensive Medicinal Chemistry III*, 694–713.

Prakoura, N., Hadchouel, J., & Chatziantoniou, C. (2019). Novel Targets for Therapy of Renal Fibrosis. *The Journal of Histochemistry and Cytochemistry : Official Journal of the Histochemistry Society*, *67*(9), 701–715.

Saleem, M. A., O'Hare, M. J., Reiser, J., Coward, R. J., Inward, C. D., Farren, T., Chang, Y. X., Ni, L., Mathieson, P. W., & Mundel, P. (2002). A conditionally immortalized human podocyte cell line demonstrating nephrin and podocin expression. *Journal of the American Society of Nephrology : JASN*, *13*(3), 630–638.

Schneider, A., Panzer, U., Zahner, G., Wenzel, U., Wolf, G., Thaiss, F., Helmchen, U., & Stahl, R. A. K. (1999). Monocyte chemoattractant protein-1 mediates collagen deposition in experimental glomerulonephritis by transforming growth factor-β. *Kidney International*, *56*, 135–144.

Sharma, K., & Ziyadeh, F. N. (1994). Renal hypertrophy is associated with upregulation of TGF-beta 1 gene expression in diabetic BB rat and NOD mouse. *The American Journal of Physiology*, *267*(6 Pt 2).

Slattery, C., Campbell, E., McMorrow, T., & Ryan, M. P. (2005). Cyclosporine A-Induced Renal Fibrosis : A Role for Epithelial-Mesenchymal Transition. *The American Journal of Pathology*, *167*(2), 395.

Sun, N., Fernandez, I. E., Wei, M., Wu, Y., Aichler, M., Eickelberg, O., & Walch, A. (2016). Pharmacokinetic and pharmacometabolomic study of pirfenidone in normal mouse tissues using high mass resolution MALDI-FTICR-mass spectrometry imaging. *Histochemistry and Cell Biology*, *145*(2), 201–211.

Sun, Y., Zhang, J., Zhang, J. Q., & Ramires, F. J. A. (2000). Local angiotensin II and transforming growth factor-beta1 in renal fibrosis of rats. *Hypertension (Dallas, Tex. : 1979)*, *35*(5), 1078–1084.

Therrien, F. J., Agharazii, M., Lebel, M., & Larivire, R. (2012). Neutralization of Tumor Necrosis Factor-Alpha Reduces Renal Fibrosis and Hypertension in Rats with Renal Failure. *American Journal of Nephrology*, *36*(2), 151–161.

Tsai, H. J., Wu, P. Y., Huang, J. C., & Chen, S. C. (2021). Environmental Pollution and Chronic Kidney Disease. *International Journal of Medical Sciences*, *18*(5), 1121.

Vaidya, S. R., & Aeddula, N. R. (2022). Chronic Renal Failure. *The Scientific Basis of Urology, Second Edition*, 257–264.

Wind, S., Schmid, U., Freiwald, M., Marzin, K., Lotz, R., Ebner, T., Stopfer, P., & Dallinger, C. (2019). Clinical Pharmacokinetics and Pharmacodynamics of Nintedanib. *Clinical Pharmacokinetics*, *58*(9), 1131.

Wollin, L., Wex, E., Pautsch, A., Schnapp, G., Hostettler, K. E., Stowasser, S., & Kolb, M. (2015). Mode of action of nintedanib in the treatment of idiopathic pulmonary fibrosis. *European Respiratory Journal*, *45*(5), 1434–1445.

Yu, A. S. L., Chertow, G. M., Luyckx, V. A., Marsden, P. A., Skorecki, K., & Taal, M. W. (2019). *Brenner and Rector's The Kidney* (11th ed.). Elsevier.

Zhou, S., Li, W., Tian, M., Zhang, N., Yang, X., Li, W., Peng, Y., & Zheng, J. (2020). Metabolic Activation of Pirfenidone Mediated by Cytochrome P450s and Sulfotransferases. *Journal of Medicinal Chemistry*, *63*(15), 8059–8068.